Submitted to JGR 15 June 2005
Accepted 22 March 2006

Attribution of recovery in lower-stratospheric ozone

Eun-Su Yang[1], Derek M. Cunnold[1], Ross J. Salawitch[2], M. Patrick McCormick[3], James Russell III[3], Joseph M. Zawodny[4], Samuel Oltmans[5], Michael J. Newchurch[6]

[1]Georgia Institute of Technology
[2]Jet Propulsion Laboratory/California Institute of Technology
[3]Hampton University
[4]NASA/Langley Research Center
[5]NOAA Earth System Research Laboratory, Global Monitoring Division
[6]University of Alabama in Huntsville

Abstract

Multiple satellite and ground-based observations provide consistent evidence that the thickness of Earth's protective ozone layer has stopped declining since 1997, close to the time of peak stratospheric halogen loading. Regression analyses with Effective Equivalent Stratospheric Chlorine (EESC) in conjunction with further analyses using more sophisticated photochemical model calculations constrained by satellite data demonstrate that the cessation of ozone depletion between 18-25 km altitude is consistent with a leveling off of stratospheric abundances of chlorine and bromine, due to the Montreal Protocol and its amendments. However, ozone increases in the lowest part of the stratosphere, from the tropopause to 18 km, account for about half of the improvement in total column ozone during the past 9 years at northern hemisphere mid-latitudes. The increase in ozone for altitudes below 18 km is most likely driven by changes in transport, rather than driven by declining chlorine and bromine. Even with this evidence that the Montreal Protocol and its amendments are having the desired, positive effect on ozone above 18 km, total column ozone is recovering faster than expected due to the apparent transport driven changes at lower altitudes. Accurate prediction of future levels of stratospheric ozone will require comprehensive understanding of the factors that drive temporal changes at various altitudes, and partitioning of the recent transport-driven increases between natural variability and changes in atmospheric structure perhaps related to anthropogenic climate change.

1. Introduction

Atmospheric ozone, which protects life on Earth's surface from damaging solar ultraviolet radiation, exists mostly (~90% of the total column) in the stratosphere. The decrease in stratospheric ozone and the character of its expected recovery have been the subject of intense research [*WMO*, 2003]. Recently reported evidence for the first stage of recovery (i.e., a slowdown in the ozone depletion rate) in the upper stratosphere at 35-45 km [*Newchurch et al.*, 2003b; *Reinsel et al.*, 2002] has confirmed our understanding of ozone chemistry and the positive effect of the Montreal Protocol and its amendments, which have led to a decline in stratospheric halogen (chlorine and bromine) loading. However, the largest fraction of the ozone column resides in the lower stratosphere, between approximately 10 and 25 km altitude [*WMO*, 1999]. The abundance of ozone in the lower stratosphere is the essential metric for confirming the health of the ozone layer.

Stratospheric ozone is continually produced by photolysis of molecular oxygen and is removed locally by both transport and chemical processes. In the upper stratosphere, transport plays a minor role and there is a direct, almost linear anti-correlation between the abundances of ozone and chlorine [e.g., figure 6-21, *WMO*, 1999]. The majority of stratospheric chlorine is supplied by industrial pollutants, such as CFCs (chlorofluorocarbons). Ozone in the lower stratosphere is sensitive to re-distribution by atmospheric transport, the abundance of volcanic aerosols, and a complex set of non-linear chemical interactions involving anthropogenic chlorine and bromine [chapter 7, *WMO*, 1999; chapter 4, *WMO*, 2003]. A number of recent studies, based on examination of time series of total column ozone, have noted a turnaround in the recent downward trend [*Reinsel et al*., 2005; *Steinbrecht et al*., 2005; *Hadjinicolaou et al*., 2005] that may be evidence for the beginning of an ozone recovery due to declining halogen loading [*Reinsel et al*., 2005]. However, *Hadjinicolaou et al*. [2005] attribute the recent turnaround in total column ozone to effects of transport. Here, we examine changes in total column ozone as well as partial ozone columns, in specific altitude regions, to better ascertain effects of halogen chemistry (i.e., chlorine and bromine) and transport forcings on recent changes in stratospheric ozone. Our focus is on changes in ozone that have occurred outside the polar regions; our analyses are

restricted to regions equatorward of 60° latitude. The long-term evolution of polar ozone is sensitive to changes in stratospheric temperature that may be linked to climate change, as well as evolving levels of chlorine and bromine, and is the subject of many other studies [*Austin et al.*, 2002; *Austin*, 2003; *Huck et al.*, 2005; *Newman et al.*, 2004; *Rex et al.*, 2004; *Shindell et al.*, 1998; *Solomon et al.*, 2005; *Yang et al.*, 2005]. However, the influence of polar ozone loss on the extra-polar ozone time series [*Reinsel et al*., 2005; *Weatherhead and Andersen*, 2005] is considered in this study.

Recently, the International Ozone Commission http://ioc.atmos.uiuc.edu/documents/Statement-QOS2004.pdf defined the first stage of ozone recovery as a 'statistically significant slowing of the downward trend'. Our study focuses on empirical evidence for this first stage of ozone recovery that is evident from several independent measurement systems and networks covering large portions of the global atmosphere during the past 25 years. These independent observing techniques show a consistent slowdown in the loss rates in total ozone columns, stratospheric ozone columns, and ozone columns between 18-25 km (near the ozone-layer maximum). Our study focuses on the attribution of changes in ozone at mid-latitudes by examining the role of chemistry and transport forcings on observed changes in partial column ozone, for layers between 18-25 km and the tropopause to 18 km. The significance of these changes is quantified by a cumulative sum of residuals analysis [*Newchurch et al.*, 2003b; *Reinsel*, 2002]. A photochemical model, constrained by satellite observations of tracers of atmospheric transport, volcanic aerosol loading, and numerous other chemical measurements, is also used to quantify the expected increases in ozone due to declining levels of stratospheric chlorine and bromine that have resulted from the Montreal Protocol and its amendments.

2. Data

The most comprehensive representation of changes in the global stratospheric ozone layer is based on the consistent results of three independent satellite instruments and two independent ground-based observing networks. We analyze the TOMS/SBUV satellite measurements to characterize total-column ozone changes from 60°S to 60°N latitudes. From the

well-calibrated ground-based networks, we use 36 Dobson/Brewer stations between 30°S-60°N to corroborate the satellite total-column ozone results. We use both SAGE and HALOE satellite measurements to characterize the global stratosphere above 18 km, between 60°S and 60°N. These ozone data are area-weighted to compute near-global mean values. Because most of the total-column ozone amount resides in the stratosphere and because the global mixing time is significantly less than the decadal time frame important here, we expect to see broadly consistent recovery signatures from all of these independent measurements.

The Stratospheric Aerosol and Gas Experiment I and II (SAGE I/II) instruments comprise the longest (1979 to August 22, 2005, but with a discontinuity between November, 1981 and October, 1984) and most widely analyzed source of global stratospheric ozone measurements [*Cunnold et al.*, 2000; *Newchurch et al.*, 2000; *WMO*, 2003]. The complete version-6.2 data set and details of the retrieval algorithm are available through http://www-sage2.larc.nasa.gov.

The version-19 Halogen Occultation Experiment (HALOE) data for 1991 to November 21, 2005 comprise a shorter, but equally accurate record of stratospheric ozone amounts, in addition to measurements of other trace gases critical to partitioning the chemical and dynamical causes of the improving ozone layer [*Russell III et al.*, 1993]. The HALOE data are available at http://haloedata.larc.nasa.gov. Both SAGE and HALOE measurements have been extensively validated [*Ackerman et al.*, 1989; *Attmannspacher et al.*, 1989; *Cunnold et al.*, 1989; *Cunnold et al.*, 1996; *Gordley et al.*, 1996; *Hervig et al.*, 1996; *Newchurch et al.*, 1995; *Oberbeck et al.*, 1989; *Russell III et al.*, 1996a,b; *Wang et al.*, 2002] and are widely accepted by the atmospheric community for studies of ozone trends [*Harris et al.*, 1998; *WMO*, 1994; *WMO*, 2003].

We also analyze global total ozone data from the merged Total Ozone Mapping Spectrometer (TOMS)/SBUV data (Merged Ozone Data, herein after referred to as the MOD), which provide nearly continuous global coverage since 1979 [*McPeters et al.*, 1996; *McPeters and Labow*, 1996; *Reinsel et al.*, 1994; *Stolarski et al.*, 1991] (details at http://code916.gsfc.nasa.gov/Data_services/merged/). Total ozone measurements observed from the ground-based Dobson [*Dobson*, 1931; *Dobson*, 1968; *Dobson and Harrison*, 1926; *Dobson et al.*, 1928; *Komhyr et al.*, 1989; *Lloyd et al.*, 1999; *Newchurch et al.*, 2000; *Staehelin et al.*, 1998;

Staehelin et al., 1995; *WMO*, 2003] and Brewer [*Bais et al.*, 1996; *Hoegger et al.*, 1992; *Kerr et al.*, 1988; *Lloyd et al.*, 1999; *McElroy and Kerr*, 1995; *Slusser et al.*, 1999; *Staehelin et al.*, 1995] spectrophotometers are obtained from the World Ozone and Ultraviolet Radiation Data Centre (WOUDC) (http://www.msc-smc.ec.gc.ca/woudc). These data are mostly selected based on table 4-4 of *WMO* [1999]: 26 Dobson/Brewer stations between 30-60°N (Kagoshima, Quetta, Sapporo, Tateno, Bismarck, Caribou, Edmonton, Arosa, Camborne, Haute Provence, Potsdam, Uccle, Vigna Di Valle, Toronto, Boulder, Belsk, Goose Bay, Churchill, Lisbon, Hradec Kralove, Hohenpeissenberg, Nashville, Wallops Island, Cairo, Sestola, and Xianghe) and 10 Dobson/Brewer stations between 30°S-30°N (Kodaikanal, New Delhi, Mauna Loa, Varanasi, Naha, Samoa, Cachoeira Paulista, Kunming, Singapore, and Natal). The selected data follow the corrections recommended by *WMO* [1999, section 4.2]. Balloon-borne ozonesonde measurements [*Newchurch et al.*, 2003a, *Oltmans et al.*, 1998; *Oltmans et al*., 1996] from 11 stations between 30-60°N (Kagoshima, Sapporo, Tateno, Edmonton, Uccle, Boulder, Goose Bay, Churchill, Hohenpeissenberg, Wallops Island, and Payerne), obtained from the WOUDC, are used to derive reliable long-term trends of ozone from the surface to 27 km [page 4.14, *WMO*, 1999]. Ozone columns are calculated both in the lower stratosphere between the tropopause and 18 km (TP-18 km) and in the middle stratosphere (18-25 km near the maximum layer in ozone concentration).

3. Statistical model

We employ a stepwise linear regression model to remove solar and Quasi Biennial Oscillation (QBO)-related signals from the ozone time series [*Newchurch et al.*, 2000; *Newchurch et al.*, 2003b]. Variations in solar ultraviolet radiation due to the 11-year cycle of solar sunspots, and changes in the direction of stratospheric winds in the tropics that vary on a roughly 2.5-year period, are known to affect measured time series of stratospheric and total column ozone. Because our emphasis is on the identification of variations in ozone due to changes in halogen loading, a statistical model is used to account for, and remove, the effects of these processes on the measured time series. Seasonal effects and the mean abundance of ozone over the time

period are also removed, providing a residual time series that is examined for evidence of ozone-layer recovery.

The linear regression model is well accepted by the atmospheric sciences community [*Harris et al.*, 1998] and is represented by

$$[O_3]_t = \mu + \omega t + [\text{Seasonal terms}] + [\text{QBO periodic terms}] + \gamma\,[F10.7]_t + U_t \qquad (1)$$

where μ is the mean level, ω is a linear trend coefficient, and the seasonal terms represent the 12-, 6-, 4-, and/or 3-months cosine terms each with a time lag to obtain the best estimate of its coefficient. The QBO periodic terms consist of an ensemble of cosines with time lags to represent the QBO signal with periods between 3 and 30 months excluding 12-, 6-, 4-, and/or 3-months terms, which are included in the seasonal coefficients. $[F10.7]_t$ is the F10.7-cm radio flux density, which is used to provide a proxy for variations in solar UV irradiance. γ is a solar signal regression coefficient. U_t is the autocorrelated error term, representing a first-order autoregressive process ($U_t = a_1 U_{t-1} + \varepsilon_t$).

Based on surface measurements of ozone depleting substances and the time lag (~3 years) involved in their rising to the altitude of the stratospheric ozone layer at mid-latitudes, we choose the start of 1997 as the time to test for an inflection in the ozone time series [*Montzka et al.*, 1999; *WMO*, 2003]. The Effective Equivalent Stratospheric Chlorine (EESC), a combined measure of lower stratospheric abundances of inorganic chlorine and bromine, peaked in mid-1996 [figure 1-23, *WMO*, 2003]. The effect of the autoregressive coefficient on the subsequent uncertainty calculation is described in the appendix. Details of the treatment of exogenous variables appear in *Newchurch et al.* [2003b].

An aerosol term is not included in the regression. Highly-elevated aerosol loading following major volcanic eruptions interferes with the space-borne measurement of lower stratospheric ozone [*Cunnold et al*., 2000]. Of course, ozone depletion results from changes in heterogeneous chemistry associated with enhanced aerosol loading following major volcanic eruptions [e.g., *Dessler et al.*, 1993; *Fahey et al*., 1993; *Wennberg et al*., 1994; *Kinnison et al*.,

1994]. Changes in stratospheric heating associated with volcanic aerosols lead to additional short-term variations in ozone [e.g., *Kinne et al*., 1992; *Kinnison et al*., 1994; *Robock*, 2000]. We have omitted data collected up to 30 months following the eruption of Mt. Pinatubo from the SAGE and HALOE time series due to the aerosol influence on space-based ozone [*Cunnold et al.*, 2000] and also because our analysis is focused on long term changes in ozone for stratospheric aerosol conditions close to background. We also omit the merged TOMS/SBUV data, Dobson/Brewer total ozone, and ozonesonde ozone records for 1991.5-1994.0 to be consistent with the statistical treatment of the SAGE and HALOE satellite records and because our study is focused on near background aerosol conditions. The omission of data for time periods perturbed by enhanced volcanic aerosols is a common practice in regression based analyses of ozone time series: e.g., *Reinsel et al*. [2005] omit data influenced by Pinatubo, as explained in paragraph 10 of their paper. Here, we show data collected during the Pinatubo time period, plotted as open circles, but we do not include these data in our statistical analyses.

4. Photochemical Model

The attribution of changes in ozone is based independently on EESC regression and on more sophisticated photochemical model calculations constrained by observations of tracers of dynamical motion and stratospheric aerosol. The EESC time series is based on measurements of tropospheric total organic chlorine (CCl_y) and bromine (CBr_y). It is lagged relative to the surface by three years [pages 1.32 and 11.15, *WMO*, 1999 and page 1.19, *WMO*, 2003]. The efficiency of ozone loss due to bromine relative to chlorine, which is based on photochemical model simulations, is used to arrive at a single time series to represent the aggregate effect of halogens on ozone [alpha factor, page 1.69, *WMO*, 2003].

Many studies which have focused on attribution of ozone changes have used EESC to represent the effects of halogens on ozone [e.g., *Newman et al.*, 2004; *Huck et al*., 2005; *Yang et al*., 2005]. However, EESC is a simplistic representation of the influence of chlorine and bromine on ozone. Not all stratospheric air is three years old, as assumed in the formulation of EESC. Also, the relative influence of chlorine and bromine on ozone loss varies as a function of altitude,

latitude, season, and aerosol loading. The formulation of EESC assumes a single relative-influence factor that has the same value at all latitudes and altitudes. However, the contribution of halogens to ozone loss varies as a function of aerosol loading [e.g., *Dessler et al.*, 1993; *Fahey et al*., 1993; *Kinnison et al*., 1994] and as a function of the abundance of HO_x (hydrogen oxide) and NO_x (nitrogen oxide) radicals. In turn, HO_x and NO_x variations are also driven by changes in H_2O, CH_4, and temperature [e.g., *Salawitch et al*., 1994; *Wennberg et al*., 1994]. Also, bromine has a larger relative influence on ozone loss near the tropopause than at higher altitudes [e.g., *Salawitch et al*., 2005].

We have used a photochemical model, constrained by satellite measurements of water vapor (H_2O), ozone (O_3), methane (CH_4), and sulfate aerosols, to compute 24-hour-average radical abundances (e.g., ClO, BrO, OH, HO_2, NO, and NO_2) for all altitudes, latitudes, and time periods under consideration. The fractional contribution of halogens to total ozone loss found from these calculated radical fields, termed $LOSS_{MODEL}$, is also used as a regression variable in the analysis discussed in Section 5. The quantity $LOSS_{MODEL}$, described more fully below, can be thought of as a more sophisticated version of EESC.

Here, we describe the procedure used to estimate $LOSS_{MODEL}$. We estimate the fraction of ozone loss due to halogens for each month of the ozone time series, at 1-km intervals between 18 and 25 km, for latitudes of 55°N, 45°N, 35°N, 5°N, 5°S, 35°S, 45°S and 55°S. The model is constrained by zonal, monthly mean values of H_2O, CH_4, and O_3, all observed by HALOE [*Russell III et al.*, 1993]. Prior to the launch of HALOE, SAGE II measurements of O_3 are used. Aerosol surface area is obtained from SAGE I and SAGE II observations [*Thomason and Poole*, 1997]. First, N_2O is calculated from HALOE zonal, monthly mean CH_4 using the formula of *Michelsen et al*. [1998]. Different relations are used for tropical and mid-latitude regions. The shapes of these relations are related to the relative lifetime of each species in the tropics and mid-latitude regions, respectively. The ATMOS relations that covered several weeks of observations at many latitudes have been shown to agree well with in situ [e.g., *Herman et al*., 1998] and aircraft [e.g., *Chang et al*., 1996a] observations of these relations, obtained at other time periods. We allowed for growth in N_2O over time of 0.315% per year, relative to 1994.875

(the time of the *Michelsen et al*. [1998] ATMOS observations), which is obtained from data in table 1-12 of *WMO* [1999]. We allowed for growth of CH_4 of 5.0 ppbv/year from 1979 until 2000 and of 2 ppbv/year from 2000 onward, again relative to 1994.875. These values are obtained from section 1.7.2 of *WMO* [2003]. These small growth rates were implemented so that the formula of *Michelsen et al.* [1998] could be incorporated more realistically into the model, which is driven ultimately by HALOE CH_4: e.g., prior to input to the *Michelsen et al.* formula, HALOE CH_4 was converted to its equivalent value for 1994.875; a value of N_2O was found using the appropriate relation, based on latitude zone; then, the computed value of N_2O was scaled to the time of the actual CH_4 observation. The growth rates for N_2O and CH_4 are a minor part of the overall analysis and have no bearing on the final results.

Inorganic chlorine (Cl_y) is estimated based on the formulation derived from aircraft measurements of organic chlorine compounds that is described by *Woodbridge et al*. [1995]. As noted above, N_2O is estimated from HALOE CH_4, using the formula from *Michelsen et al*. [1998], allowing for the small temporal growth in both N_2O and CH_4 described above. For the estimate of Cl_y, the following relation with N_2O was used:

$$[Cl_y] = 3.53876 - 2.57709\times10^{-3}\,[N_2O] - 1.91693\times10^{-5}\,[N_2O]^2 - 2.40584\times10^{-8}\,[N_2O]^3 \quad (2)$$

where $[Cl_y]$ and $[N_2O]$ are in ppbv. This relation is based on in situ measurements of a complete set of halocarbons obtained during the SOLVE campaign [*Schauffler et al.*, 2003]. All other aspects of the computation of Cl_y are based on the method described by *Woodbridge et al.* [1995], which allows for Cl_y to be computed for earlier time periods by adjusting the value of total chlorine in the troposphere [equation 11 of *Woodbridge et al.*, 1995].

Inorganic bromine (Br_y) is estimated based on a relation derived from aircraft measurements of the bromocarbon source gases and nitrous oxide (N_2O) [*Wamsley et al.*, 1998]. For the estimate of Br_y, a correlation with CFC-11 is used, because the primary bromine source gas, CH_3Br, has a stratospheric lifetime somewhat similar to lifetime of CFC-11 [e.g., plate 1 of *Wamsley et al.*, 1998). Equations 15 and 16 of *Wamsley et al.* [1998] are used to estimate CFC-11 from N_2O, based on whether data was obtained in the tropics of extratropics, respectively.

We allow for variations in the age of air in the calculation of Cl_y and Br_y, as outlined by *Woodbridge et al*. [1995] and *Wamsley et al*. [1998], using the relation between age and N_2O given in figure 2.12 of *Park et al*. [1999]. This relation between age of air and N_2O is very similar to an independent determination reported by *Engel et al*. [2002]. Finally, the temporal evolution of CCl_y and CBr_y, which appear as factors in the formula for Cl_y and Br_y [e.g., *Woodbridge et al*., 1995; *Wamsley et al*., 1998], is based on the WMO 2003 Ab baseline scenario [e.g., table 1-16, *WMO*, 2003]. This method for estimating Cl_y and Br_y from tracers has been used in many empirical studies of balloon and aircraft data [e.g., *Chang et al*., 1996a; *Salawitch et al*., 1994; *Salawitch et al*., 2005 and references therein] and is a common tool for estimating time series of halogens [e.g., *Engel et al*., 2002].

A second set of calculations was conducted for the tropical region. The use of HALOE CH_4 to prescribe model Cl_y and NO_y for 18 to 25 km in the tropics is a challenge, because measured CH_4 lies close to its tropopause value. Hence, small uncertainties in measured CH_4 can lead to large relative errors in estimated Cl_y and NO_y. For this second set of calculations, model HCl and NO_x was constrained to match the zonal, monthly mean HALOE observations of these quantities by adjusted model Cl_y and NO_y to match the data. Both sunrise and sunset observations were used, with the model matching the appropriate time of observation. Model Br_y was scaled to preserve the Cl_y to Br_y ratio for the particular time of observation. Monthly mean values of Cl_y, Br_y, and NO_y, normalized to year 1993.0, were computed for each latitude region over the UARS time period. These monthly mean values were propagated backwards in time to cover the time period between 1979 and the first data from HALOE, using the known temporal changes in organic chlorine, organic bromine, and N_2O (e.g., WMO 2002 Ab scenario for CCl_y and CBr_y, augmented by constant values of CH_2Br_2 and CH_2BrCl for Br_y; NO_y growth of 0.315% per year, based on the N_2O growth described above).

Estimates of NO_y are based on its relation with N_2O. For values of N_2O < 150 ppb, we use the formula of *Rinsland et al*. [1999]. For N_2O > 150 ppb, the relation of *Popp et al*. [2001] is used. The *Rinsland et al*. [1999] relation is based on measurements from ATMOS; the *Popp et al*. [2001] relation is based on data from aircraft and balloons. The relation between NO_y and N_2O is

robust, displaying small variations outside the polar regions [e.g., *Sen et al*., 1998; *Keim et al*., 1997]. Indeed, various coupled climate and chemistry models, as well as 2D and 3D models, display much larger variations in the NO_y vs N_2O relation (compared to either other models, or to data) than is commonly seen in measurements from different instruments [e.g., *Chang et al*., 1996b; *Park et al*., 1999]. The good agreement between measured and modeled NO_x, illustrated in Figure 1, again provides confidence in the fidelity of this approach. As for HCl, excellent agreement is found for altitudes above 19 km. At 19 km and lower altitudes, small measurement uncertainties in CH_4 have a large affect on the model results, because the tracer-tracer relations are approaching tropopause values that lie close to zero. Similar comparisons between measured and modeled NO_x are found for other latitudes (not shown).

The model is constrained by observations of CH_4 and H_2O, which are important for calculating HO_x radicals. For the UARS time period, zonal, monthly mean observations from HALOE are used. For the pre-UARS time period, we propagated back in time the monthly mean value of H_2O, for the specific latitude and altitude point, derived from HALOE measurements and assuming zero trend for H_2O. A similar treatment is used for CH_4, except we allow for the small temporal trend noted above. In other words, for all Januaries prior to the launch of UARS, the same value of H_2O is used for the model grid point in question (function of altitude and latitude), which is derived from a mean of all model grid points (at the same altitude and latitude) for times when data are available. The trends in H_2O are uncertain, particularly prior to the launch of UARS [*SPARC*, 2000]. However, the scientific results of this paper, the attribution of changes in ozone to the leveling off of Cl_y and Br_y, are insensitive to any reasonable assumption regarding dH_2O/dt over the pre-UARS time period. The reason for this insensitivity is that the abundance of HO_x varies in proportion to changes in the square root of the concentration of H_2O. Finally, there are occasional gaps in monthly, zonal mean HALOE and SAGE II data due to the sampling of the respective instruments. For these occasions, which are rare in the overall analysis, values of $LOSS_{MODEL}$ are not computed, and this information is treated is “not available” in the CUSUM analysis of these model results.

Figure 1 compares modeled and measured HCl (sunrise and sunset) and NO_x (sunset) at 20 and 25 km, for three latitude regions. The good agreement between modeled and measured HCl and NO_x demonstrates the reliability of the approach. A model calculation for the tropics, based on specification of Cl_y and NO_y from measured CH_4, tends to simulate HCl and NO_x reasonably well at 25 km (not shown). However, this model overestimates both HCl and NO_x at 20 km, because the HALOE CH_4 time series lies close to tropopause values of CH_4, which introduces uncertainties in estimates of Cl_y and NO_y based on this "tracer-tracer" approach. Hence, for the tropics, we show here and use in our CUSUM analysis the model calculation constrained to match HALOE HCl and NO_x. The resulting CUSUMs of $LOSS_{MODEL}$ for both of these calculations in the tropics are remarkably similar, however, as discussed in Section 5.

Finally, since we are using the formula of *Wamsley et al.* [1998] to derive Br_y, the derived values are ~2.4 ppt higher than values that would be derived from consideration of supply of bromine from only CH_3Br and halons. Here, we assume CH_2Br_2 and CH_2BrCl are constant over time. The values of Br_y in this model are smaller than values inferred from some measurements of BrO [e.g., *Salawitch et al.*, 2005], possibly due to an important role for stratospheric supply of bromine from biogenic bromocarbons. However, the role of biogenic bromocarbons on stratospheric Br_y is a subject of active research [e.g., *Salawitch*, 2006]: retrievals of BrO from SCIAMACHY by one group suggest a modest role for this source [*Sinnhuber et al.*, 2005], in line with the approach used here, whereas retrievals from another group suggest a much larger role for biogenic bromine [*Sioris et al.*, 2006]. An attempt to model the role of biogenic bromocarbons is beyond the scope of this paper, although in Section 5 we comment about the possible affect of these compounds on the attribution of ozone changes in the lowermost stratosphere.

Our approach allows us to calculate how ozone loss by halogens has evolved over time in response to changes in chlorine, bromine, water, methane, HO_x, NO_x, and sulfate aerosol loading as well as variations in atmospheric transport. Changes in transport are reflected in changes in CH_4, which controls the input fields of NO_y, Cl_y, and Br_y. This model has been shown to provide accurate simulations of hydrogen, nitrogen, and chlorine radical species under a variety of aerosol loading, seasonal, and latitudinal conditions [*Osterman et al.*, 1997; *Salawitch*,

2002; *Sen et al.*, 1999; *Sen et al.*, 1998]. Model results are integrated from 18 to 25 km, weighted by the concentration of ozone at each altitude. Similar results are found if we were to use equal weights for each altitude (this weighting is almost identical to a non-weighted average because the ozone contents of each 1-km layer are almost all equal). The resulting time series is referred to as $Loss_{MODEL}$. Plots of $Loss_{MODEL}$ for 7 latitude bands centered between 60°S and 60°N are shown in Figure 2. The calculated increase in ozone loss by halogens between 1979 and 2005 is consistent with the overall rise in stratospheric chlorine and bromine loading (top panel, Figure 2). However, ozone loss by halogens peaked near 1992, which is expected based on known photochemistry in the presence of highly elevated abundances of stratospheric aerosol following the eruption of Mt. Pinatubo [*Dessler et al.*, 1993; *Fahey et al.*, 1993]. Figure 2 shows results for $LOSS_{MODEL}$ in the tropics (10ºS to 10ºN) for the model constrained by measured HCl and NO_x, which is a more accurate empirical approach for this region of the atmosphere, where the tracer-tracer relation approach introduces some uncertainty. Interestingly, however, nearly identical results for $LOSS_{MODEL}$ are found for the tropics using the tracer-tracer approach. Ozone loss in the tropics is found from a balance between halogen and HO_x photochemistry and decreases in H_2O and CH_4 measured by HALOE since ~2002 result in the points for $LOSS_{MODEL}$, for the past 4 years, lying above the blue curve (EESC fit to $LOSS_{MODEL}$) by comparable amounts for both simulations.

An outstanding scientific issue, which is not addressed in our study, is that even though the effect of enhanced chemical loss of ozone due to Pinatubo aerosols is readily apparent from various ozone datasets in the Northern Hemisphere, this same affect is not apparent from measurements in ozone obtained in the Southern Hemisphere [section 4.6.6, *WMO*, 2003]. The reason for this disparity is a subject of active research and is especially puzzling given the large, Pinatubo induced decline in column NO_2 observed at Lauder, New Zealand [e.g., figure 4-21, *WMO*, 2003]. We avoid this confounding issue by omitting in our analysis data collected during times of highly perturbed aerosol loading.

Two time series are used independently for the attribution of ozone loss by halogens: values of EESC (Figure 2) from *WMO* [2003] Ab baseline scenario and values of $Loss_{MODEL}$. The

EESC time series allows observed changes in O_3 to be related to well-established variations in the abundance of stratospheric halogens. The $Loss_{MODEL}$ time series is a refinement to the EESC-based estimate, allowing the changes in O_3 to be related to the time evolution of ozone loss by halogens accounting for "age of air" as well as observed changes in CH_4, H_2O, aerosol loading, NO_x and HO_x radicals, in addition to variations in Cl_y and Br_y.

5. Changes in ozone trends

The three left panels in Figure 3 show the residual ozone time series from SAGE and HALOE (top), Dobson/Brewer spectrophotometers (middle), and the merged TOMS/SBUV satellite instruments (bottom) that remain after the mean, seasonal, QBO, and solar terms have been removed, as described in Equation (1). The excellent agreement between the SAGE and HALOE measurements of the temporal evolution of stratospheric ozone is apparent in the top left panel. Likewise, the linear trends from 1979.0 to the end of 1996 (=1997.0) from SAGE (–2.3 ± 0.2 %/decade with 2σ uncertainty), Dobson/Brewer (–2.1 ± 0.5 %/decade), and the MOD (–1.6 ± 0.3 %/decade) are consistent over a broad portion of Earth's atmosphere.

We calculate the cumulative departure of the measured ozone from the 1979-1996 trend line (solid black line) extended forward to the time period 1997 to 2005, using the cumulative sum (CUSUM) of residuals technique [*Newchurch et al.*, 2003b; *Reinsel*, 2002]. If there is less ozone depletion after 1997 than before, then ozone residuals after 1997 will show systematic positive values above the projected trend line (black dotted line). The 95% confidence limits for unbiased residuals appear as the black dotted traces in the right panels of Figure 3, where the limits increase with time due to unresolved fluctuations and uncertainty in the trend estimates.

If the autocorrelation of the error terms (i.e., the AR(1) term) is significant, two problems are expected in the ordinary least-squares fittings [e.g., see (8-56) and (8-60) of *Johnston*, 1984]: (1) The estimated trend (ω) is unbiased, but the standard deviation for ω is underestimated and (2) the variance of U_t is also underestimated. The underestimation of the variance of U_t is not serious in this study because of the relatively large sampling size. The variances of mean level and trend estimates, however, should be corrected by a correction factor (cf) = $(1+r)/(1-r)$, where r

is an autocorrelation parameter. In addition, the cumulative residuals tend to have more dispersion in the presence of a positive autocorrelation. Therefore, the variance of the cumulative ozone residuals (predicted) is calculated as (see Appendix),

$$\mathrm{VAR}\{\mathrm{CUSUM}\}$$

$$= \mathrm{VAR}\{\mathrm{CUSUM\ residuals}\} + n_2^2 * \mathrm{VAR}\{\mathrm{mean}\} + [\Sigma_2 (t - t_o)]^2 * \mathrm{VAR}\{\mathrm{trend}\}$$

$$\approx cf \cdot \sigma^2 \{n_2 + n_2^2 / n_1 + [\Sigma_2 (t - t_o)]^2 / \Sigma_1 (t - t_o)^2\},$$

where σ is a standard error of the residuals for 1979-1996, n_1 is number of data before the turnaround point (1997.0), n_2 is number of data after the turnaround point, t_o is the mean value of t for 1979-1996 [see *Newchurch et al*., 2003b]. The estimated autocorrelation parameters are ~0.5 for the MOD and ~0.4 for the ground Dobson/Brewer data in this study, resulting in inflations of CUSUM uncertainties by ~70% and ~50% for the MOD and Dobson/Brewer data. However, the autocorrelation parameter for the SAGE ozone residuals above 18 km is 0.08 so that its trend and CUSUM uncertainty are much less affected by these autoregressive processes. We expect the AR(1) parameter to be larger in the total ozone column than in the stratospheric column above 18 km because of the altitude dependence of the ozone lifetime (decreasing with altitude).

The CUSUMs plotted in the right panels of Figure 3 for the corresponding measurements are by definition equal to zero at the start of 1997; the small fluctuations prior to 1997 represent deviations from an assumption of linear ozone depletion over time. The CUSUMs increase starting in 1997.0, rising significantly above the 95% confidence limits indicated by the black dotted envelope for years after 1997. For example, the CUSUM metric for the SAGE data is 76% at the end of data (2005.5), while a CUSUM of only 29% would be considered a 2σ departure from the extended linear trend line if ozone loss over the 1979-1996 and 1997-2005 time periods had occurred at the same rate. The green parabolic traces show the expected CUSUM behavior for ozone levels held constant after 1997.0. The recovery signatures from both the

Dobson/Brewer networks and the MOD are highly significant, and reflect increases in total column ozone since 1997. The Dobson/Brewer and MOD CUSUM values are larger than the SAGE value, because the SAGE value is based on data acquired only above 18 km altitude. As we show below, the region between the tropopause and 18 km (TP-18 km) contributes significantly to trends in total column ozone. Recognizing the 2-sigma uncertainty envelopes shown on Figure 3, we find that taken together, these independent measurements provide compelling evidence that, outside of the polar regions, the decline in stratospheric ozone above 18 km has slowed down significantly since the beginning of 1997 and the decline in total-column ozone has stopped entirely.

Figure 4 shows the SAGE/HALOE residual ozone time series between 18-25 km, for northern mid-latitudes (30-60°N, top panels), tropics (10°S-10°N, middle panels), and southern mid-latitudes (30-60°S, bottom panels). Because the HALOE ozone measurements are less sensitive to aerosol loadings than the SAGE measurements, this combined ozone data set consists of SAGE data before the Pinatubo eruption and HALOE data after the eruption. The regression of the EESC time series (top panel, Figure 2) onto these ozone time series results in the corresponding blue lines, representing an estimate of the ozone changes resulting from the cessation of increasing levels of stratospheric halogens that occurred in approximately 1997. The time series in the left panels and the CUSUM metrics in the right panels indicate close correspondence between the observed ozone changes (black traces) and this estimate of ozone changes due to the halogen loading (blue traces), for all three latitude regions.

Further confirmation that the changes in the ozone time series between 18-25 km are due to changes in halogen loading is provided by model estimates of the fraction of ozone loss due to halogens ($Loss_{MODEL}$) over the time period 1979 to present. The regression of $Loss_{MODEL}$ onto the ozone time series is shown by the red lines on the left hand panels of Figure 4. The CUSUM of the regression is shown by the red lines on the right panels. For northern and southern mid-latitudes, the CUSUMs for the SAGE/HALOE ozone time series, for EESC, and for $Loss_{MODEL}$ provide an overall consistent picture of a change in linear trend near 1997, consistent

with the time of peak halogen loading. The slight sensitivity of these results to the year of change in linear trend (1997 is used here) is described below.

The only deviation from this consistent picture is apparent, but with fewer data points, for the tropical region from 2001 to present. Here, the CUSUM for residual ozone displays a lag of ~2 years relative to the CUSUM for EESC (black and blue lines, middle right panel, Figure 4). Notably, the CUSUM for $LOSS_{MODEL}$ indicates that little change in the fractional loss of ozone due to halogens is expected (red curve) between 1979 and present. This behavior of $LOSS_{MODEL}$ is driven by a smaller relative contribution of halogens to total ozone loss compared to the other latitude regions, because in the tropical lower stratosphere, inorganic chlorine and bromine have yet to be fully released from their organic reservoirs. Loss of ozone by HO_x radicals exerts the predominant chemical influence, and trends in ozone are sensitive to both dynamics and changes in H_2O and CH_4. As noted above, similar CUSUM curves for $LOSS_{MODEL}$ in the tropics are found using a tracer-tracer approach, rather than the more empirical approach (e.g., model constrained by measured HCl and NO_x) used for the curve shown in Figure 4. The disagreement between CUSUMs for $LOSS_{MODEL}$ and EESC suggests a simple regression of residual ozone would not be appropriate for the tropical lower stratosphere. This appears to be borne out by the ozone time series, which does not display a statistically significant change in linear trend as is seen in the other regions. Furthermore, time series of zonal, monthly mean HALOE H_2O and CH_4 in the tropics exhibit significant long-term variability, with a tendency towards lower values since ~2002. The HALOE H_2O and CH_4 data suggest the tropical lower stratosphere has undergone significant recent change in the effect of both transport and thermodynamics on its overall composition.

To establish attribution of the improving ozone conditions, we examine measurements of ozone collected in various altitude regions. Three altitude regions are considered: tropopause to 18 km, 18 to 25 km, and 25 km to the top of the atmosphere (TOA). Here, only data acquired in the northern hemisphere mid-latitudes are shown. Changes in ozone as a function of altitude in southern hemisphere mid-latitudes are challenging to define because SAGE I measurements below 18 km altitude are unreliable (in both hemispheres) and Lauder ozonesonde observations start in 1987. Figure 5 shows changes in ozone at 30-60°N for the three altitude regions noted

above, compared in this case to time series of EESC. The change in EESC is consistent with the measured ozone behavior in the 18-25 km layer. This correspondence strongly suggests that chemistry related to EESC changes, as opposed to dynamical changes, has been responsible for the ozone changes in this layer. The correspondence between EESC and the ozone time series and CUSUMs in Figure 4 support this conclusion.

Table 1 summarizes the estimated trends in ozone for the three altitude regions between 30-60°N, as well as the total column, based on various data sets. The decline in total column ozone from 1979-1996 was −9.3 ± 3.3 (2σ) DU/decade in the MOD record and −8.7 ± 2.3 (2σ) in the Dobson/Brewer networks (Table 1). Ozonesondes yield a value of −2.1 ± 1.6 DU/decade for the change between the tropopause and 18 km. Trends of ozone in the 18-25 km layer are −3.9 ± 0.9 based on only SAGE I/II, −4.7 ± 1.3 DU/decade based on the ozonesonde time series, and −4.4 ± 1.2 DU/decade using the SAGE/HALOE record (all uncertainties throughout are 2σ estimates). From 25 km to the TOA, SAGE indicates −4.3 ± 1.0 DU/decade was lost. Hence, we find that ~20% of the decline of total ozone from 1979-1996 was due to changes between the tropopause and 18 km, 38% of the drop occurred between altitudes of 18-25 km, and 42% of the change occurred above 25 km.

The altitude partitioning of the improvement in the stratospheric ozone layer starting in 1997 is significantly different from the altitude partitioning of the decline (Table 1). The same data sets described above yield an improvement in total ozone column of 16.3 ± 6.6 DU/decade from 1997-2005 with respect to the declining trend line, with 49% of the improvement occurring between the tropopause and 18 km, 21% between altitudes of 18-25 km, and 30% due to ozone increases above 25 km.

The ozone changes in the tropopause to 18 km layer since 1997.0, as shown in Figure 5 (bottom panel) and Table 1, are much larger than can be explained by known chemistry (i.e., the EESC fit accounts for only approximately 50 CDU of the calculated 389 CDU change, where CDU is cumulative DU). An analysis based on $Loss_{MODEL}$, using known photochemistry and established tracer relations, similarly fails to account for the observed features of the ozone time series (not shown). We should expect that some of the ozone change in the lower layer since 1997 results

from a change in the flux from the source layer above, because of the chemically induced ozone change in the 18-25 km layer, even if there is no change in the dynamics. Based on an ozone change of 249 CDU in the 18-25 km layer (average of 167 for SAGE, 309 for SAGE/HALOE and 271 for ozonesondes, see Table 1), and because there is approximately twice as much ozone in this layer as in the tropopause to 18 km layer, a change of perhaps 124 CDU in the lower layer might be related to this change of the downward flux without any change in the dynamics. Combining this change with the EESC effect falls significantly short of accounting for the observed change of 389 CDU relative to the pre-1997 trend. Therefore, transport changes probably dominate the changes in ozone from 1997 to 2005, between the tropopause and 18 km, for the 30-60°N region.

Because of the slowly-varying changes in ozone depleting substances at the ground and the effect of mixing (which induces a spectrum to the mean age of air) [e.g., *Waugh et al*., 2001; *Engel et al*., 2002], the expected turnaround point for ozone cannot be precisely defined. Figure 6 illustrates the sensitivity of the analysis to variations in the turnaround year, for residuals at 18-25 km, 30-60°N, for SAGE ozone (left panels) and ozonesonde ozone (right panels) residuals. The late turnaround points in 1998 and 1999 result in more precise trend estimates and less uncertainty of the CUSUM envelopes, which are balanced by the smaller CUSUM values due to the smaller number of time steps for CUSUM calculations. Nonetheless, for turnaround in 1998 or 1999, the CUSUMs for SAGE and ozonesonde residuals approach or exceed the 95% confidence intervals (black dotted lines) at the end of the time period. Assuming a turn around point of 1995.0 (top panels, Figure 6) is the only case where the CUSUM values fails to exceed the 95% confidence interval. In this case, the turn around point is close to the discontinuity caused by the data exclusion during the Pinatubo period. Figure 6, therefore, shows shifts of the turn around time by about one year forward from 1997.0, or two years after 1997.0, do not change the conclusions of this study.

6. Relative roles of transport and chemistry

Support for the inferred relative roles of chemistry and transport in producing the observed ozone changes since 1997.0 is provided by results shown in Figures 7 through 9. The residual column ozone at 18-25 km and TP-18 km in Figure 5 has significant periodicities of 3-5 years. In order to show a clear long-term change in ozone, these ENSO-like signals are removed from the ozone time series [e.g., *Steinbrecht et al*., 2005] only in Figures 7 and 8 in this study. Figure 7 displays results of the regression of EESC, temperature (T), tropopause height (TPH), and potential vorticity (PV) onto residual ozone values smoothed with a 13-month filter. The temperature, tropopause height, and potential vorticity are calculated at the same locations and times as the ozonesonde measurements, using NCEP reanalysis data. The cause of long term changes in temperature and tropopause height is difficult to assess, since each is sensitive to climate change as well as ozone depletion [e.g., *Santer et al*., 2003]. Indeed, *Santer et al*. [2003] estimate, based on a climate model simulation, that declining ozone is the largest contributor to rising tropopause height over the 1979 to 1999 time period. However, rising levels of greenhouse gases are also expected to lead to significant increases in tropopause height. The changes in PV illustrated in Figure 7 are likely indicative of changes in Rossby wave breaking events that can clearly affect ozone time series in this region of the atmosphere [e.g., *Koch et al*., 2002]. However, PV can also change due to variations in static stability, and hence is not uncoupled from changes in tropopause height and temperature.

The analysis shown in Figure 7 indicates that variations of temperature, tropopause height and PV explain more of the ozone variance from 1979 to 2005 in the lower layer (tropopause to 18 km) than they explain in the 18 to 25 km region. The overall percentage of the ozone variance explained by EESC, relative to T, TPH, and PV is much larger for the 18-25 km region than the TP-18 km layer. However, as noted above, variations in T, TPH, and PV could be due to feedbacks related to ozone changes, or could be driven by changes in transport ultimately related to climate change.

To further explore the factors responsible for observed variations in ozone at different atmosphere levels, we examine the relation between these quantities over shorter time periods.

Figure 8, using a 3-month filter on ozone residuals, shows the close correspondence of ozone with T, TPH, and PV on time scales of a few months. We tested several proxies and found that except for ENSO, their influences on the long-term changes in ozone at 18-25 km are negligible, although the other proxies have some effects on the ozone below 18 km. The overall higher correlations of T, TPH, and PV with ozone residuals below 18 km, relative to the correlation with EESC, when residuals are examined for short term fluctuations provides further evidence that changes in ozone below 18 km are not driven by halogen chemistry. The weak correlations between these dynamical variables and ozone above 18 km, relative to the correlation of O_3 with EESC, suggests a weak contribution from changes in dynamics (or climate) to long-term changes in ozone above 18 km. Similarly, the weak correlation between EESC and ozone below 18 km shown in Figure 8 is indicative of small contribution of ClOx/BrOx chemistry to the long-term change in ozone below 18 km. Although temperature explains 48% and 38% of ozone variance at 18-25 km in Figures 7 and 8, the linear decrease of temperature over the entire time period does not match the curved shape of the ozone residual at 18-25 km. The linear decrease of temperature over time, different in shape from the ozone time series, seems consistent with forcing from both changes in ozone and rising levels of greenhouse gases [e.g., *Santer et al*., 2003].

It has been suggested that the turnaround year of 1997 might pose a complication due to a number of cold Arctic winters that began in this time period [*Weatherhead and Andersen*, 2005]. To investigate the influence of polar ozone loss on the extra-polar ozone time series, we examine the relation between residual ozone and the volume of air in the Arctic vortex exposed to polar stratospheric clouds (V_{PSC}). It has been shown that V_{PSC} is a good proxy for chemical loss of Arctic ozone [*Rex et al*., 2004; *Tilmes et al*., 2004; *Chipperfield et al*., 2005]. Figure 9 compares the time series of residual ozone for various altitudes and latitudes, as indicated, to a time series for V_{PSC} that is based on the same data points for each panel. The values of V_{PSC} are calculated in the same manner as described by *Rex et al*. [2004]. The regressions of SAGE ozone residuals with V_{PSC} appear as blue for regions showing negative correlations and are plotted as negative values to visually emphasize the correlation; red is used for regions showing positive correlations

between residual ozone and V_{PSC}. A negative correlation between V_{PSC} and residual ozone means that larger values of chemical loss of polar ozone are associated with decreases in the ozone abundance at mid-latitudes, as hypothesized by *Weatherhead and Andersen* [2005]. Figure 9 shows the region of strong, negative correlations between V_{PSC} and SAGE ozone variations for 50-60°N, below ~16 km. These results suggest horizontal transport of chemically depleted ozone from the Arctic vortex might account for some of the observed negative trends in ozone for this region of the atmosphere. But, this influence appears to be confined mainly to altitudes below ~16 km, and latitudes poleward of 50°N. The regressions shown in Figure 9 demonstrate that, for the majority of the extra-polar data considered here, the dominant changes in ozone are not driven by polar ozone chemical loss.

Hadjinicolaou et al. [2005] state "all of the observed upward trend [in total column ozone from MOD] from 1994 to 2003 are reproduced by the [SLIMCAT] model which is forced only by transport changes" [e.g., halogen levels are fixed at 1980's levels]. This finding appears at first glance to be different from our results, which require both chemical and dynamical forcings to reproduce measured ozone residuals since 1997. Figure 1 and figure 2a in *Hadjinicolaou et al*. [2005] show that (1) the negative trend in total column ozone for 1979-1993 is mostly due to the increasing halogen loading for the same period and (2) the transport changes along with fixed halogen loading is mostly responsible for the rise in column ozone for 1994-2003. Their results, as shown in their figure 2a in particular, appear to us to require the existence of a substantial change in halogen loading, between 1980 and 1994, in order to explain the changes in column ozone over the entire time period. Note that their model with fixed halogen loading is predicting larger ozone values in 2003 than in 1980, which is contrary to observations shown here.

Positive changes in ozone since 1996 were also obtained from the MOD, SBUV(/2), and Dobson/Brewer total ozone data by *Reinsel et al*. [2005], who showed that the changes were significant both with and without the dynamical considerations. Their result indicates that the changes in total column ozone are attributable to chemistry as well as dynamics. Our study compliments the analysis of *Reinsel et al*. [2005] by showing that the positive trend in ozone since

1996/1997 results both from the transport driven increases in ozone for the tropopause to 18 km layer and from predominantly chemical driven increases in ozone for altitudes above 18 km.

Finally, *Salawitch et al.* [2005] noted that bromine supplied to the stratosphere from biogenic bromine and tropospheric BrO could lead to larger amounts of ozone depletion, between the tropopause and ~18 km, compared to models that consider supply of bromine only from CH_3Br and halons. The effect of biogenic bromine on ozone trends is most notable during time of elevated aerosol loading (figure 4 of *Salawitch et al.*). During periods of background loading, ClO levels are too small, below 18 km, for ozone loss by the BrO+ClO cycle to be efficient. We have conducted simulations using constant offsets to the Br_y relation based on the WMO Baseline Ab scenario for CH_3Br and halons (not shown), and the resulting values of $LOSS_{MODEL}$ are unable to reproduce the large increases in ozone observed below 18 km since 1997. It is important to note that these simulations assumed constant offsets to Br_y (e.g., that the supply of bromine from short lived, biogenic bromocarbons and tropospheric BrO is constant over time). If the supply of biogenic bromine to the stratosphere had varied over time, with a strong decrease after 1997, then ozone levels would be expected to rise, due to the $BrO+HO_2$ cycle (figure 5 of *Salawitch et al.*). However, values of Br_y inferred from balloon observations of BrO appear to exhibit a near constant offset relative to the bromine content of CH_3Br+halons, data that spans stratospheric entry dates of 1992 to 2002 [figure 1-8 of WMO, 2003; Dorf, 2005]. Therefore, we consider it unlikely that biogenic bromine could be responsible for the rise in ozone observed between 18 km and the tropopause since 1997.

We conclude that observed ozone changes in the 18-25 km layer since 1979 are consistent with chemical effects driven by increases in halogens. However, increases in ozone observed after 1997 between the tropopause and 18 km likely have had a significant transport component. About half of the observed increase in ozone since 1997 has occurred between the tropopause and 18 km.

7. Conclusions

Analyses of monthly stratospheric and total-column ozone values from three independent satellite instruments and two ground-based networks of sensors comprising combinations of the SAGE I/II, HALOE, merged TOMS/SBUV satellites, the Dobson/Brewer ground-based networks, and the global ozonesonde network indicate that the thickness of Earth's stratospheric ozone layer stopped declining after about 1997. Regression analyses of both EESC (effective equivalent stratospheric chlorine) and of more sophisticated photochemical calculations independently indicate that the temporal signature of the observed changes in ozone above 18 km altitude is consistent with the timing of peak stratospheric halogen abundances, which occurred mid-way through 1997. These results confirm the positive effect of the Montreal Protocol and its amendments on limiting the growth of stratospheric chlorine and bromine, and in protecting Earth's ozone layer.

Increases in stratospheric ozone at NH mid-latitudes since the mid-1990s are also observed for altitudes below 18 km. These increases appear to be driven principally by changes in atmospheric dynamics. The changes in ozone for this height region exhibit positive correlations with dynamical proxies such as potential vorticity and tropopause height, and do not bear the signature of expected long-term change due to stratospheric halogens. The rise in total column ozone since 1997, for NH mid-latitudes (30–60°N), appears to be caused by ~50% contribution from increases in ozone below 18 km altitude, and ~50% contribution from rising ozone above 18 km. Hence, both chemical and dynamical forcings appear to be responsible for the observed rise in column ozone at NH mid-latitudes since 1997. Much work remains in order to understand whether the dynamically driven changes are due to natural variability or due to changes in atmospheric structure related to anthropogenic climate change. Furthermore, the recent observations of stratospheric ozone were obtained during a time of unusually low levels of stratospheric aerosol loading. Chemical reactions initiated by volcanic aerosol that penetrates the stratosphere, should a major eruption occur, will almost certainly lead to short periods of lower ozone due to ozone destruction by anthropogenic halogens in the presence of those aerosols.

We conclude by noting that our paper represents the complete data record from the remarkable SAGE and HALOE instruments. SAGE I commenced observations in 1979 and SAGE II ceased operating on August, 22 2005. HALOE ceased operating on December 14, 2005. The SAGE I/II and HALOE instruments documented ozone depletion due to rising CFCs, the start of the recovery of ozone (above 18 km) due to declining CFCs, and an unanticipated significant increase in ozone since 1997 (between the tropopause and 18 km) due most likely to changes in stratospheric transport. The data record provided by HALOE and SAGE played an important role in quantifying the effect of human activity on the ozone layer that led to the passage of the Montreal Protocol and its amendments that restricted the production of CFCs.

Acknowledgements. The solar data were obtained from the NOAA National Geophysical Data Center, ftp://ftp.ngdc.noaa.gov/STP/SOLAR_DATA/SOLAR_RADIO/FLUX/. This research including the SAGE, HALOE, TOMS, and SBUV programs was supported by NASA and NOAA. Ozonesonde observations are supported by many national research programs worldwide. Research at the Jet Propulsion Laboratory, California Institute of Technology, is performed under contract with National Aeronautics and Space Administration. SAGE and HALOE data for this study were obtained from the NASA/LaRC data center. Dobson/Brewer total ozone and ozonesonde ozone data were provided by the World Ozone and Ultraviolet Data Center (WOUDC) in Toronto, Canada and by the Swiss Meteorological Service. The merged TOMS/SBUV data were provided by NASA/GFSC. EESC data were provided by S. Montzka/NOAA/CMDL. We thank the three reviewers for their helpful comments and constructive criticism, and Markus Rex for sharing values of V_{PSC} used in this study. This work is dedicated to the memory of Professor Greg Reinsel.

Figure Captions

Figure 1. Comparison of modeled and measured HCl and NO_x. Time series of zonal, monthly mean HCl and NO_x measured by HALOE (black circles) at 20 and 25 km, for indicated latitude regions, compared to calculated values of HCl and NO_x (red dots). Data and model results for HCl include sunrise and sunset points. Data and model results for NO_x are shown only for sunset. The comparisons for sunrise (not shown) are comparable, but both measured and modeled NO_x are lower than sunset values, due to the diurnal cycle of NO_x. The simulations for the equatorial regions are constrained to measured HCl and NO_x during the UARS time period (Cl_y and NO_y are adjusted in the model); for earlier time periods, monthly mean values of Cl_y and NO_y normalized to 1993 are propagated backwards, using the known temporal changes in organic chlorine and N_2O.

Figure 2. Time series of Equivalent Effective Stratospheric Chlorine, EESC, (upper) and fractional ozone loss rate due to halogens (lower). The fractional ozone loss rate ($Loss_{MODEL}$) results from photochemical model calculations that are constrained by observations as described in the text. Fractional ozone loss rate is the ozone loss rate due to halogens divided by total ozone loss rate integrated from 18 to 25 km weighted by the ozone concentrations at each altitude in 7 latitude bands. The blue lines show the EESC series fitted to the fractional loss rates whose data are excluded during the Pinatubo period.

Figure 3. Time series of monthly average ozone residuals plus linear trend (left) and cumulative sum (CUSUM) of residuals (right) in % for the SAGE(black)/HALOE(red) stratospheric ozone columns above 18 km between 60°S-60°N (top panels), Dobson/Brewer total ozone columns 30°S-60°N (middle panels), and merged TOMS/SBUV (MOD) total ozone columns 60°S-60°N (bottom panels). The SAGE, HALOE, Dobson/Brewer, and merged TOMS/SBUV monthly residuals are all independently obtained by removing the seasonal, solar, and QBO terms from their respective ozone series. The trend line indicates the

ozone trend calculated from observations for 1979-1996 (solid line) and forecasted linearly afterward (dotted line). Linear trends and 95% confidence intervals for 1979-1996 are listed. The ozone residuals during the Pinatubo period are shown in open circles, but they are excluded from the trend calculations. The last value in the cumulative residual time series represents the cumulative difference of all monthly residuals after 1997.0 with respect to the predicted trend line. The green line represents the hypothetical case where the ozone values remained at their 1997.0 value until 2005. The black dotted lines in the right panels indicate the 95% confidence envelopes of departure from natural variability and model uncertainty.

Figure 4. Time series of monthly ozone residuals plus linear trend (black trace in the left panels) and cumulative sum of residuals (black trace in the right panels) for the SAGE/HALOE data integrated from 18 to 25 km for 30-60°N (top panels), 10°S-10°N (middle panels), and 30-60°S (bottom panels).Tabulated trends correspond to 1979-1996 (black line in left panels) projected to 2005 (dotted black lines, left panels). The SAGE data are used for the period before the Pinatubo volcanic eruptions and HALOE data afterwards. The blue lines represent the ozone change estimated by the EESC fit (left) and its cumulative sum (right). The red lines show the ozone evolution expected from the photochemical calculations (left panels) and the cumulative sum of the ozone change estimated by the calculated fractional loss rate (right panels). The black dotted lines in the right panels indicate the 95% confidence envelopes of departure from natural variability and model uncertainty

Figure 5. Time series of monthly ozone residuals plus linear trends from SAGE (red traces in the left panels) and ozonesondes (black traces) at 30-60°N; cumulative sum in the right panels in DU. Top panels display SAGE I/II values above 25 km and the associated EESC fit. Middle panels display ozonesonde values from 11 stations (black), SAGE I/II (red) and EESC fit (blue) at 18-25 km. The ozone residuals during the El Chichon and

Pinatubo period are shown in open circles, but they are excluded from the trend calculations. Bottom panels display ozonesonde values (black) and SAGE II (red) with EESC fit to ozonesonde values (blue) between tropopause and 18 km.

Figure 6. CUSUM calculations for the SAGE (left panels) and ozonesonde (right panels) ozone residuals between 18-25 km, 30-60°N. The turnaround points are selected at 1995.0, 1996.0, 1997.0, 1998.0, and 1999.0 (top to bottom panels, respectively).

Figure 7. Ozonesonde residuals plus trend (black traces) between tropopause-18 km (left panels) and 18-25 km (right panels) when additional ENSO-like signals (periodicities of 31-60 months) are removed from the ozonesonde measurements between 30-60°N in Figure 5. Similarly, the respective residuals are calculated for temperature, tropopause height, and potential vorticity. These residuals are smoothed by a 13-month running mean to show their long-term changes. The ozone residuals are separately regressed against the EESC series (first panel) and temperature residuals (second panel), tropopause-height residuals (third panel), and potential-vorticity residuals (fourth panel). The estimated ozone responses are shown in blue lines for EESC, T, TPH, and PV, respectively. The percentage of the ozone variance explained individually by the exogenous variable is shown in the individual panels.

Figure 8. Same as in Figure 7, but smoothed by a 3-month (instead of 13-month) running mean to show the short-term fluctuations of ozone, EESC, temperature, tropopause height, and potential vorticity.

Figure 9. Time series of the volume of polar stratospheric air containing Polar Stratospheric Clouds (Vpsc) and SAGE ozone residuals at 50-60°N, 40-50°N, and 30-40°N from 10 to 24 km. The ozone residuals for March and April are regressed onto the Vpsc values. The negative of the Vpsc series is plotted when the correlations are negative (blue line) in

order to visually emphasize the correlations. The negative correlation coefficient is significant only below 18 km at 50-60°N.

Table 1. Altitude distribution of decreasing trends, uncertainties, and fractional altitude partitioning (1979-1996) from five different ozone records between 30-60°N and corresponding average accumulation rates**, uncertainties, and altitude partitioning (1997-2005).

Altitude Range	Instrument	Trend 1979-1996 [DU/decade]	Trend Uncertainty 2σ	% of Total 1979-1996	CUSUM 1997-2005 CDU(2σ)	Average Accumulation Rate [DU/decade]	Accumulation Rate Uncertainty 2σ	% of Total 1997-2005
25 km-TOA	SAGE	–4.3	1.0	42	238 (141)*	4.9	2.9	30
18-25 km	Ozonesonde	–4.7	1.3		271 (206)	5.6	4.2	
	SAGE	–3.9	0.9	38	167 (138)*	3.4	2.8	21
	SAGE/HALOE	–4.4	1.2		309 (174)*	6.4	3.6	
	Average	–4.3	0.7			5.1		
TP-18 km	Ozonesonde	–2.1	1.6	20	389 (256)	8.0	5.3	49
Σ layers	SAGE/ SAGE/sonde	–10.3	2.1		794 (323)	16.3	6.6	
Total Column	D/B	–8.7	2.3		845 (399)	17.4	8.2	
	MOD	–9.3	3.3					

*mean ozone deviations assumed for missing data points.

**The CUSUM value is the cumulative (consecutive) sum of the ozone residual deviations from the projected trend line in the left panels of Figures 3 through 5. For a 1979-1996 trend estimate of ω_1, assuming a linear trend, ω_2, after 1997.0, the ozone deviations from the 1979-1996 trend line will follow the line, $(\omega_2-\omega_1) * t$, with random fluctuations. Therefore, $[CUSUM]_t$ = Integral of $(\omega_2-\omega_1) * t = ½ * (\omega_2-\omega_1) * t^2$, where t is months. For example, $[CUSUM]_t$ = 309 CDU at t = 108 months (9 years * 12 months/year) in the upper panel of Figure 4. Then, $309 = ½ * (\omega_2-\omega_1) * t^2$ and $(\omega_2-\omega_1)$ = 6.4 DU/decade. With ω_1 = –4.4 DU/decade in Figure 4, ω_2 = 2.0 DU/decade. Therefore, the 1997-2005 average accumulation rate estimated by the CUSUM value is +2.0 DU/decade. This result is not a trend calculation, but rather an average accumulation rate with the starting point (1997.0) fixed to the value of 1979-1996 trend line at 1997.0 with all data are equally weighted. From this argument, however, it is clear that the change in trend at 1997.0 is proportional to the CUSUM value.

Appendix:

When the error terms in the regression model are positively correlated, the ordinary least squares (OLS) estimates suffer the following two problems (e.g., *Johnston*, 1984).

1. The estimated regression coefficients are unbiased, but their error estimates could be underestimated.
2. The variance of ozone residuals is underestimated.

The second problem is not serious in this study because of large sampling size (~200). The variance of a cumulative sum of residuals, however, increases due to a positive autocorrelation of ozone residuals (see Section C).

A. AR(1) term in time series data

The typical trend model for ozone can be described as

$$[O_3]_t = c + \omega t + \alpha [S]_t + \beta [QBO]_t + \gamma [Solar]_t + U_t \qquad \text{(A1)}$$

where c and ω are constant and linear trend terms and $[S]_t$, $[QBO]_t$, and $[Solar]_t$ represent ozone variations due to season, QBO, and solar variations, respectively. Ozone trend plus error terms are now obtained by subtracting season, QBO, and solar variations from the original ozone time series, leading to the following expression:

$$[O_3]_t' = c + \omega t + u_t \qquad \text{(A2)}$$

where $u_t = \rho\, u_{t-1} + \varepsilon_t$ and ε_t is a white noise process (i.e., sequential errors are independent of each other). Even after removing ozone signals with phase (seasonal, QBO, and solar terms), the error term often shows a first-order autoregressive process, AR(1). The autocorrelated disturbance could be attributed mostly to missing explanatory variables, misspecification of the

form of regression, or characteristics of a data set. If the AR(1) parameter, ρ, is positive, the estimates (c and ω) in Equation (A2) are unbiased but their standard errors are underestimated [e.g., *Pindyck and Rubinfeld*, 1998].

In particular, at t-1, the above ozone series can be written as

$$[O_3]_{t-1}' = c + \omega(t-1) + u_{t-1}. \tag{A3}$$

Then,

using $u_t = \rho u_{t-1} + \varepsilon_t$,

$$[O_3]_t' - c - \omega t = \rho\{[O_3]_{t-1}' - c - \omega(t-1)\} + \varepsilon_t.$$

When introducing transformed variables, $[O_3]^*_t$, c*, and t*, we obtain

$$[O_3]_t^* = c^* + \omega^* t^* + \varepsilon_t \tag{A4}$$

where

$[O_3]_t^* = [O_3]_t' - \rho\,[O_3]_{t-1}' = (1-\rho B)\,[O_3]_t'$,

$c^* = c\,(1-\rho) = (1-\rho B)\,c$,

$t^* = t - \rho\,(t-1) = (1-\rho B)\,t$, and

B is a backward shift operator, i.e., $B[O_3]_t' = [O_3]_{t-1}'$.

In order to estimate the autocorrelation parameter ρ, we use the Hildreth-Lu procedure which minimizes the error sum of squares in the transformed regression model (A4) [*Neter et al.*, 1996]. The estimate of ρ is denoted here as r. The transformation reported by (A4) is the same as the transformation used by the Yule-Walker procedure [*Pankratz*, 1983] and the results obtained here are similar to the results obtained using that procedure.

B. Variance of CUSUM without an AR(1) term

If there is no AR(1) term in the regression model (A2), and if the ozone trend after the turnaround point (T_o) is the same as that before T_o (same-trend hypothesis), the variance of the predicted ozone time series ($[O_3]_{t'}$) after T_o is [*Makridakis et al*., 1983; *Draper and Smith*, 1998]:

Variance of predicted $[O_3]_{t'}$

= VAR{residuals} + VAR{mean estimate} + VAR{trend estimate}

$$= \sigma_u^2 \{1 + 1 / n_1 + (t - \tau_1)^2 / \Sigma_1(t - \tau_1)^2\}. \qquad \text{(B1)}$$

where

VAR{residuals} = σ_u^2,

VAR{mean estimate} = σ_u^2 / n_1,

VAR{trend estimate} = $\sigma_u^2 / \Sigma_1(t - \tau_1)^2 = \sigma_u^2 / [(t_1 - \tau_1) + (t_2 - \tau_1) + \ldots + (t_{n1} - \tau_1)]^2$,

n_1 = number of data prior to T_o,

n_2 = number of data from T_o onward,

τ_1 = mean value of t prior to T_o, and

τ_2 = mean values of t after T_o.

The first term in the right hand side of Equation (B1) arises from random noise and the second and third terms result from uncertainties in regression coefficients of mean and trend estimates.

The variance of CUSUM is a variance of the cumulative predicted-$[O_3]_t'$ such that

CUSUM variance of predicted $[O_3]_t'$

$$= E[\{\Sigma_2 ([O_3]_t' - E[O_3]_t'])\}^2]$$

$$= n_2 \cdot VAR\{residuals\} + n_2^2 \cdot VAR\{mean\ estimate\} + \Sigma_1(t - \tau_1)^2 \cdot VAR\{trend\ estimate\}$$

$$= \sigma_u^2 \{n_2 + n_2^2 / n_1 + [\Sigma_2 (t - \tau_1)]^2 / \Sigma_1(t - \tau_1)^2\}, \qquad \text{(B2)}$$

where n_1 is the number of data prior to T_o and E[x] is the expected value of x. The variance of CUSUM after T_o increases with t, t^2, and t^4 due to random fluctuations, uncertainty in mean level, and uncertainty in trend estimate, respectively [*Newchurch et al.*, 2003b].

C. CUSUM variance with an AR(1) term

If the residuals are correlated in an AR(1) process, the regression model (A2) does not provide the correct uncertainty in the trend estimate. Instead, the regression model (A4) estimates an unbiased standard error of the ozone trend. Comparing models (A2) and (A4), we can see that the independent variable t* converges to t when $r \rightarrow 0$. Since we are interested in ozone variations for actual time step (t), (A4) divided by (1-rB) leads to,

$$[O_3]_t' = c^*/1-r + \omega^* t + \varepsilon_t/(1-rB) \qquad \text{(A4′)}$$

VAR{predicted $[O_3]_t'$}

= VAR{residuals} + VAR{mean estimate} + VAR{trend estimate}

$$\approx \sigma_u^2 \{1 + 1 / n_1 \cdot cf + (t - \tau_1)^2 / \Sigma_1(t - \tau_1)^2 \cdot cf\} \qquad \text{(B1′)}$$

where

$\sigma_u^2 = \sigma_\varepsilon^2 / (1-r^2)$ from the relation $u_t = \rho\, u_{t-1} + \varepsilon_t$,

VAR{residuals} = VAR{ε_t / (1-rB)} = VAR{$(1 + rB + r^2B^2 + r^3B^3 + \ldots)\varepsilon_t$} = $\sigma_\varepsilon^2 / (1-r^2)$,

VAR{mean estimate} = $\sigma_\varepsilon^2 / (1-r)^2 / n_1$, = $\sigma_u^2 \cdot (1-r^2) / (1-r)^2 / n_1 = cf \cdot \sigma_u^2 / n_1$,

VAR{trend estimate} = $\sigma_\varepsilon^2 / \sum(t^*)^2 = \sigma_\varepsilon^2 / [(1-r)^2 \sum(t)^2] = cf \cdot [\sigma_\varepsilon^2 / (1-r^2)] / \sum(t)^2$,

and cf = (1+r) / (1-r).

Due to the positive autocorrelations seen in most ozone time series, the ozone residuals in the next step tend to follow the previous residual disturbances, resulting in more dispersion from their expectation value. Indeed, a larger variance of CUSUM residuals is estimated if the autocorrelation parameter r is positive.

At $t = n_1 + 1$ (first data point after T_o),

$E[u_t \cdot u_t]$

$= E[(\varepsilon_{n1+1} + r\,\varepsilon_{n1} + r^2\,\varepsilon_{n1-1} + r^3\,\varepsilon_{n1-2} + \ldots) \cdot (\varepsilon_{n1+1} + r\,\varepsilon_{n1} + r^2\,\varepsilon_{n1-1} + r^3\,\varepsilon_{n1-2} + \ldots)]$

$= E[(\varepsilon_{n1+1}^2 + r^2\,\varepsilon_{n1}^2 + r^4\,\varepsilon_{n1-1}^2 + r^6\,\varepsilon_{n1-2}^2 + \ldots)]$

$= \sigma_\varepsilon^2 + r^2\,\sigma_\varepsilon^2 + r^4\,\sigma_\varepsilon^2 + r^6\,\sigma_\varepsilon^2 + \ldots$

$= 1 \cdot \sigma_\varepsilon^2 / (1-r^2)$

At $t = n_1 + 2$ (second data point after T_o),

$E[(u_t + u_{t-1}) \cdot (u_t + u_{t-1})]$

$= E[\{(\varepsilon_{n1+2} + r\,\varepsilon_{n1+1} + r^2\,\varepsilon_{n1} + r^3\,\varepsilon_{n1-1} + \ldots) + (\varepsilon_{n1+1} + r\,\varepsilon_{n1} + r^2\,\varepsilon_{n1-1} + r^3\,\varepsilon_{n1-2} + \ldots)\} \cdot \{(\varepsilon_{n1+2} + r\,\varepsilon_{n1+1} + r^2\,\varepsilon_{n1} + r^3\,\varepsilon_{n1-1} + \ldots) + (\varepsilon_{n1+1} + r\,\varepsilon_{n1} + r^2\,\varepsilon_{n1-1} + r^3\,\varepsilon_{n1-2} + \ldots)\}]$

$= E[(\varepsilon_{n1+2}^2 + (1+r)^2\,\varepsilon_{n1+1}^2 + r^2\,(1+r)^2\,\varepsilon_{n1}^2 + r^4\,(1+r)^2\,\varepsilon_{n1-1}^2 + \ldots)]$

$= \sigma_\varepsilon^2 + (1+r)^2 / (1-r^2) \cdot \sigma_\varepsilon^2$

$= (2+2r) \cdot \sigma_\varepsilon^2 / (1-r^2)$

At $t = n_1 + 3$ (third data point after T_o),

$E[(u_t + u_{t-1} + u_{t-2}) \cdot (u_t + u_{t-1} + u_{t-2})]$

$= E[\{(\varepsilon_{n1+3} + r\,\varepsilon_{n1+2} + r^2\,\varepsilon_{n1+1} + r^3\,\varepsilon_{n1} + \ldots) + (\varepsilon_{n1+2} + r\,\varepsilon_{n1+1} + r^2\,\varepsilon_{n1} + r^3\,\varepsilon_{n1-1} + \ldots) + (\varepsilon_{n1+1} + r\,\varepsilon_{n1} + r^2\,\varepsilon_{n1-1} + r^3\,\varepsilon_{n1-2} + \ldots)\} \cdot \{(\varepsilon_{n1+3} + r\,\varepsilon_{n1+2} + r^2\,\varepsilon_{n1+1} + r^3\,\varepsilon_{n1} + \ldots) + (\varepsilon_{n1+2} + r\,\varepsilon_{n1+1} + r^2\,\varepsilon_{n1} + r^3\,\varepsilon_{n1-1} + \ldots) + (\varepsilon_{n1+1} + r\,\varepsilon_{n1} + r^2\,\varepsilon_{n1-1} + r^3\,\varepsilon_{n1-2} + \ldots)\}]$

$= E[(\varepsilon_{n1+3}^2 + (1+r)^2\,\varepsilon_{n1+2}^2 + (1+r+r^2)^2\,\varepsilon_{n1+1}^2 + r^2\,(1+r+r^2)^2\,\varepsilon_{n1}^2 + r^4\,(1+r+r^2)^2\,\varepsilon_{n1-1}^2 + \ldots)]$

$= \sigma_\varepsilon^2 + (1+r)^2 \cdot \sigma_\varepsilon^2 + (1+r+r^2)^2 / (1-r^2) \cdot \sigma_\varepsilon^2$

$= (3+4r+2r^2) \cdot \sigma_\varepsilon^2 / (1-r^2)$

At $t = n_1 + 4$ (fourth data point after T_o),

$E[(u_t + u_{t-1} + u_{t-2} + u_{t-3}) \cdot (u_t + u_{t-1} + u_{t-2} + u_{t-3})]$

$= E[\{(\varepsilon_{n1+4} + r\,\varepsilon_{n1+3} + r^2\,\varepsilon_{n1+2} + r^3\,\varepsilon_{n1+1} + \ldots) + (\varepsilon_{n1+3} + r\,\varepsilon_{n1+2} + r^2\,\varepsilon_{n1+1} + r^3\,\varepsilon_{n1} + \ldots) + (\varepsilon_{n1+2} + r\,\varepsilon_{n1+1} + r^2\,\varepsilon_{n1} + r^3\,\varepsilon_{n1-1} + \ldots) + (\varepsilon_{n1+1} + r\,\varepsilon_{n1} + r^2\,\varepsilon_{n1-1} + r^3\,\varepsilon_{n1-2} + \ldots)\} \cdot \{(\varepsilon_{n1+4} + r\,\varepsilon_{n1+3} + r^2\,\varepsilon_{n1+2} + r^3\,\varepsilon_{n1+1} + \ldots) + (\varepsilon_{n1+3} + r\,\varepsilon_{n1+2} + r^2\,\varepsilon_{n1+1} + r^3\,\varepsilon_{n1} + \ldots) + (\varepsilon_{n1+2} + r\,\varepsilon_{n1+1} + r^2\,\varepsilon_{n1} + r^3\,\varepsilon_{n1-1} + \ldots) + (\varepsilon_{n1+1} + r\,\varepsilon_{n1} + r^2\,\varepsilon_{n1-1} + r^3\,\varepsilon_{n1-2} + \ldots)\}]$

$= E[(\varepsilon_{n1+4}^2 + (1+r)^2 \varepsilon_{n1+3}^2 + (1+r+r^2)^2 \varepsilon_{n1+2}^2 + (1+r+r^2+r^3)^2 \varepsilon_{n1+1}^2 + r^2 (1+r+r^2+r^3)^2 \varepsilon_{n1}^2 + r^4 (1+r+r^2+r^3)^2 \varepsilon_{n1-1}^2 + \ldots)]$

$= \sigma_\varepsilon^2 + (1+r)^2 \cdot \sigma_\varepsilon^2 + (1+r+r^2)^2 \cdot \sigma_\varepsilon^2 + (1+r+r^2+r^3)^2 / (1-r^2) \cdot \sigma_\varepsilon^2$

$= (4+6r+4r^2+2r^3) \cdot \sigma_\varepsilon^2 / (1-r^2)$

.

.

.

At $t = n_1 + n2$ (last data point),

$E[(u_t + u_{t-1} + u_{t-2} + u_{t-3} + \ldots) \cdot (u_t + u_{t-1} + u_{t-2} + u_{t-3} + \ldots)]$

$= E[\{(\varepsilon_{n1+n2} + r\, \varepsilon_{n1+n2-1} + r^2 \varepsilon_{n1+n2-2} + r^3 \varepsilon_{n1+n2-3} + \ldots) + (\varepsilon_{n1+n2-1} + r\, \varepsilon_{n1+n2-2} + r^2 \varepsilon_{n1+n2-3} + r^3 \varepsilon_{n1+n2-4} + \ldots) + \ldots\} \cdot \{(\varepsilon_{n1+n2} + r\, \varepsilon_{n1+n2-1} + r^2 \varepsilon_{n1+n2-2} + r^3 \varepsilon_{n1+n2-3} + \ldots) + (\varepsilon_{n1+n2-1} + r\, \varepsilon_{n1+n2-2} + r^2 \varepsilon_{n1+n2-3} + r^3 \varepsilon_{n1+n2-4} + \ldots) + \ldots\}]$

$= E[(\varepsilon_{n1+n2}^2 + (1+r)^2 \varepsilon_{n1+n2-1}^2 + (1+r+r^2)^2 \varepsilon_{n1+n2-2}^2 + \ldots + (1+r+r^2+\ldots+ r^{n2})^2 \varepsilon_{n1+1}^2 + r^2 (1+r+r^2+\ldots+ r^{n2})^2 \varepsilon_{n1}^2 + r^4 (1+r+r^2+\ldots+ r^{n2})^2 \varepsilon_{n1-1}^2 + \ldots)]$

$= \sigma_\varepsilon^2 + (1+r)^2 \cdot \sigma_\varepsilon^2 + (1+r+r^2)^2 \cdot \sigma_\varepsilon^2 + (1+r+r^2+r^3)^2 \cdot \sigma_\varepsilon^2 + \ldots + (1+r+r^2+\ldots+ r^{n2})^2 / (1-r^2) \cdot \sigma_\varepsilon^2$

$= \{n_2 + 2\,(n_2-1)\, r + 2\,(n_2-2)\, r^2 + 2\,(n_2-3)\, r^3 + \ldots + 2\,(1)\, r^{n2-1}\} \cdot \sigma_\varepsilon^2 / (1-r^2)$

$\approx \{n_2 + 2\, n_2\, r / (1-r)\} \cdot \sigma_\varepsilon^2 / (1-r^2)$

$= n_2 \cdot (1+r) / (1-r) \cdot \sigma_\varepsilon^2 / (1-r^2)$

$= \sigma_\varepsilon^2 / (1-r^2) \cdot n_2 \cdot cf$

Because of the sufficiently large number of n_2 in this study (108 months from 1997 to 2005), the variance of the CUSUM residuals approaches $\sigma_\varepsilon^2 / (1-r^2) \cdot n_2 \cdot cf$. Therefore, the variance of the CUSUM is calculated as

VAR{cumulative predicted-$[O_3]_{t'}$}

= VAR{CUSUM residuals} + $n_2^2 \cdot$ VAR{mean estimate} + $[\Sigma_2\, (t - \tau_1)]^2 \cdot$ VAR{trend estimate}

$$\approx cf \cdot \sigma_u^2 \{n_2 + n_2^2 / n_1 + [\Sigma_2 (t - \tau_1)]^2 / \Sigma_1 (t - \tau_1)^2\} \qquad (B2')$$

In the above derivations, we neglect uncertainty in an estimated r. Compared to the CUSUM variances without an AR(1) term, (B2′) now shows that the variances increase by a correction factor, (1+r)/(1-r).

References

Ackerman, M., et al., European validation of SAGE II aerosol profiles, *J. Geophys. Res.*, *94* (D6), 8399-8411, 1989.

Andersen, S. B., et al., Comparison of recent modeled and observed trends in total column ozone, *J. Geophys. Res.,* accepted, 2005.

Attmannspacher, W., J. de la Noe, D. de Muer, J. Lenoble, G. Megie, J. Pelon, P. Pruvost, and R. Reiter, European validation of SAGE II ozone profiles, *J. Geophys. Res.*, *94*, 8461-8466, 1989.

Austin, J., N. Butchart, and K. Shine, Possibility of an Arctic ozone hole in a doubled-CO_2 climate, *Nature*, *360*, 221-225, 1992.

Austin, J., et al., Uncertainties and assessments of chemistry-climate models of the stratosphere, *Atmospheric Chemistry and Physics*, *3* (1), 1-27, 2003.

Bais, A.F., C.S. Zerefos, and C.T. McElroy, Solar UVB measurements with the double- and single- monochromator Brewer Ozone Spectrophotometers, *Geophys. Res. Lett.*, *23* (8), 833-836, 1996.

Chang, A. Y., et al., A comparison of measurements from ATMOS and instruments aboard the ER-2 aircraft: Tracers of atmospheric transport, *Geophys. Res. Lett*., *23*, 2389-2392, 1996a.

Chang, A. Y., et al., A comparison of measurements from ATMOS and instruments aboard the ER-2 aircraft: Halogenated gases, *Geophys. Res. Lett*., *23*, 2393-2396, 1996b.

Chipperfield, M. P., W. Feng, and M. Rex, Arctic ozone loss and climate sensitivity: Updated three-dimensional model study, *Geophys. Res. Lett*., *32*, L11813, doi:10.1029/2005GL022674, 2005.

Cunnold, D.M., W.P. Chu, R.A. Barnes, M.P. McCormick, and R.E. Veiga, Validation of SAGE II ozone measurements, *J. Geophys. Res.*, *94*, 8447-8460, 1989.

Cunnold, D.M., L. Froidevaux, J.M. Russell, B. Connor, and A. Roche, Overview of UARS ozone validation based primarily on intercomparisons among UARS and Stratospheric Aerosol and Gas Experiment II measurements, *J. Geophys. Res.*, *101* (D6), 10,335-10,350, 1996.

Cunnold, D .M., M. J. Newchurch, L. E. Flynn, H. J. Wang, J. M. Russell, R. McPeters, J. M. Zawodny, and L. Froidevaux, Uncertainties in upper stratospheric ozone trends from 1979 to 1996, *J. Geophys. Res.*, *105* (D4), 4427-4444, 2000.

Dessler, A. E., et al., Balloon-borne measurements of ClO, NO and O3 in volcanic cloud: An analysis of heterogeneous chemistry between 20 and 30 km, *Geophys. Res. Lett.*, *20* (22), 2527-2530, 1993.

Dobson, G.M.B., A photoelectric spectrophotometer for measuring the amount of atmospheric ozone, *Proc. Phys. Soc., London*, *43*, 324-339, 1931.

Dobson, G.M.B., Forty years' research on atmospheric ozone at Oxford: A history, *Applied Optics*, *7*, 387-405, 1968.

Dobson, G.M.B., and D.N. Harrison, Measurements of the amount of ozone in the Earth's atmosphere and its relation to other geophysical conditions, *Proc. R. Soc. London A*, *110*, 660-693, 1926.

Dobson, G.M.B., D.N. Harrison, and J. Lawrence, Measurements of the amount of ozone in the Earth's atmosphere and its relation to other geophysical conditions, *Proc. R. Soc. London A*, *122*, 456-486, 1928.

Dorf, M., Investigations of inorganic stratospheric bromine using balloon-borne DOAS measurements and model simulations, doctoral dissertation, Univ. of Heidelberg, Heidelberg, Germany, 2005.

Draper, Norman R. and Harry Smith, Applied Regression Analysis, 3rd ed., John Wiley & Sons, New York, N. J., 1998.

Engel A., M. Strunk, M. Müller, H.-P. Haase, C. Poss, I. Levin, and U. Schmidt, Temporal development of total chlorine in the high-latitude stratosphere based on reference distributions of mean age derived from CO_2 and SF_6, *J. Geophys. Res*., 107 (D12), 4136, doi:10.1029/2001JD000584, 2002.

Fahey, D. W., et al., In situ measurements constraining the role of sulphate aerosols in mid-latitude ozone depletion, *Nature*, *363*, 509-514, 1993.

Gordley, L. L., et al., Validation of nitric oxide and nitrogen dioxide measurements made by the Halogen Occultation Experiment for UARS platform, *J. Geophys. Res.*, *101* (D6), 10,241-10,266, 1996.

Hadjinicolaou, P., J. A. Pyle, and N. R. P. Harris, The recent turnaround in stratospheric ozone over northern middle latitudes: A dynamical modeling perspective, *Geophys. Res. Lett.*, *32*, L12821, doi:10.1029/2005GL022476, 2005.

Harris, N., R. Hudson, and C. Phillips, SPARC/IOC/GAW Assessment of Trends in the Vertical Distribution of Ozone, in *World Climate Research Programme of WMO/ICSU*, pp. 289 pp., 1998.

Herman, R. L., et al., Tropical entrainment timescales inferred from stratospheric N_2O and CH_4 observations, *Geophys. Res. Lett*., *25*, 2781-2784, 1998.

Hervig, M.E., J.M. Russell III, L.L. Gordley, J.H. Park, S.R. Drayson, and T. Deshler, Validation of aerosol measurements from the Halogen Occultation Experiment, *J. Geophys. Res.*, *101* (D6), 10,267-10,275, 1996.

Hoegger, B., G. Levrat, J. Staehelin, H. Schill, and P. Ribordy, Recent developments of the Light Climatic Observatory - ozone measuring station of the Swiss Meteorological Institute (LKO) at Arosa, *J. Atmos. Terr. Phy.*, *54*, 497-505, 1992.

Huck P. E., A. J. McDonald, G. E. Bodeker, and H. Struthers, Interannual variability in Antarctic ozone depletion controlled by planetary waves and polar temperature, *Geophys. Res. Lett*., *32*, L13819, doi:10.1029/2005GL022943, 2005.

Johnston, J., *Econometric methods*, 3rd ed., McGraw-Hill, New York, 1984.

Keim, E. R., et al., Measurements of the NO_y-N_2O correlation in the lower stratosphere: Latitudinal and seasonal changes and model comparisons, *J. Geophys. Res*., *102*, 13193, 1997.

Kerr, J.B., I.A. Asbridge, and W.F.J. Evans, Intercomparison of total ozone measured by the Brewer and Dobson spectrophotometers at Toronto, *J. Geophys. Res.*, *93* (D9), 11,129-11,140, 1988.

Kinne, S., O. B. Toon, and M. J. Prather, Buffering of stratospheric circulation by changing amounts of tropical ozone: a Pinatubo case study, *Geophys. Res. Lett.*, *19*, 1927-1930, 1992.

Kinnison, D. E., K. E. Grant, P. S. Connell, D. A. Rotman, and D. J. Wuebbles, The chemical and radiative effects of the Mount Pinatubo eruption, *J. Geophys. Res.*, *99*, 25705-25731, 1994.

Koch, G., H. Wernli, J. Staehelin, and T. Peter, A Lagrangian analysis of stratospheric ozone variability and long-term trends above Payerne (Switzerland) during 1970–2001, *J. Geophys. Res.*, 107 (D19), 4373, doi:10.1029/2001JD001550, 2002.

Komhyr, W.D., R.D. Grass, and R.K. Leonard, Dobson spectrophotometer 83: A standard for total ozone measurements, 1962-1987, *J. Geophys. Res.*, *94*, 9847-9861, 1989.

Lloyd, S., et al., Intercomparison of total ozone observations at Fairbanks, Alaska, during POLARIS, *J. Geophys. Res.*, *104* (D21), 26,767-26,778, 1999.

Makridakis, Spyros, Steven C. Wheelwright, and Victor E. McGee, Forecasting: Methods and Applications, 2nd ed., John Wiley & Sons, New York, N. J., 1983.

McElroy, C.T., and J.B. Kerr, Table mountain ozone intercomparison: Brewer ozone spectrophotometer Umkehr observations, *J. Geophys. Res.*, *100*, 9293-9300, 1995.

McPeters, R.D., S.M. Hollandsworth, L.E. Flynn, J.R. Herman, and C.J. Seftor, Long-term ozone trends derived from the 16-year combined Nimbus 7/Meteor 3 TOMS Version 7 record, *Geophys. Res. Lett.*, *23* (25), 3699-3702, 1996.

McPeters, R.D., and G.J. Labow, An assessment of the accuracy of 14.5 years of Nimbus 7 TOMS Version 7 ozone data by comparison with the Dobson network, *Geophys. Res. Lett.*, *23* (25), 3695-3698, 1996.

Michelsen, H.A., G.L. Manney, M.R. Gunson, C.P. Rinsland, and R. Zander, Correlation of stratospheric abundances of CH_4 and N_2O derived from ATMOS measurements, Geophys. Res. Lett., 25 (15), 2777-2780, 1998.

Montzka, S.A., J.H. Butler, J.W. Elkins, T.M. Thompson, A.D. Clarke, and L.T. Lock, Present and future trends in the atmospheric burden of ozone-depleting halogens, *Nature*, *398*, 690-694, 1999.

Neter, J., M. H. Kutner, C. J. Nachtsheim, and W. Wasserman, Applied Linear Statistical Models, 4th ed., McGraw-Hill, 1996.

Newchurch, M. J., M. A. Ayoub, S. Oltmans, B. Johnson, and F. J. Schmidlin, Vertical Distribution of Ozone at Four Sites in the United States, *J. Geophys. Res.*, *108(D1)* (doi:1029/2002JD001059), 4031, 2003a.

Newchurch, M. J., et al., Upper-stratospheric ozone trends 1979-1998, *J. Geophys. Res.*, *105* (D11), 14,625-14,636, 2000.

Newchurch, M.J., D.M. Cunnold, and H.J. Wang, Stratospheric Aerosol and gas experiment II - Umkehr ozone profile comparisons, *J. Geophys. Res.*, *100* (D7), 14,029-14,042, 1995.

Newchurch, M.J., E.-S. Yang, D.M. Cunnold, G.C. Reinsel, J.M. Zawodny, and J.M.R. III, Evidence for Slowdown in Stratospheric Ozone Loss: First Stage of Ozone Recovery, *J. Geophys. Res.*, *108 (D16)* (doi:10.1029/2003JD003471), 4507, 2003b.

Newman, P.A., S. R. Kawa, and E. R. Nash, On the size of the Antarctic ozone hole, *Geophys. Res. Lett.*, *31* (L21104, doi:10.1029/2004GL020596), 2004.

Oberbeck, V.R., J.M. Livingston, P.B. Russell, R.F. Pueschel, J.N. Rosen, M.T. Osborn, M.A. Kritz, K.G. Snetsinger, and G.V. Ferry, SAGE II aerosol validation: selected altitude measurements, including particle micromeasurements, *J. Geophys. Res.*, *94* (D6), 8367-8380, 1989.

Oltmans, S.J., A.S. Lefohn, H.E. Scheel, J.M. Harris, H. Levy II, I.E. Galbally, E.-G. Brunke, C.P. Meyer, J.A. Lathrop, B.J. Johnson, D.S. Shadwick, E. Cuevas, F.J. Schmidlin, D.W. Tarasick, H. Claude, J.B. Kerr, O. Uchino, and V. Mohnen, Trends of ozone in the troposphere, Geophys. Res. Lett., 25 (2), 139-142, 1998.

Oltmans, S.J., H. Levy II, J.M. Harris, J.T. Merrill, J.L. Moody, J.A. Lathrop, E. Cuevas, M. Trainer, M.S. O'Neill, J.M. Prospero, H. Vomel, and B.J. Johnson, Summer and spring

ozone profiles over the North Atlantic from ozonesonde measurements, J. Geophys. Res., 101 (D22), 29,179-29,200, 1996.

Osterman, G.B., R.J. Salawitch, B. Sen, G.C. Toon, R.A. Stachnik, H.M. Pickett, J.J. Margitan, J.-F. Blavier, and D.B. Peterson, Balloon-borne measurements of stratospheric radicals and their precursors: Implications for the production and loss of ozone, *Geophys. Res. Lett.*, *24* (9), 1107-1110, 1997.

Pankratz, A., Forecasting with Univariate Box-Jenkins models: concepts and cases, 562 pp, New York, 1983.

Park, J. H., M. K. W. Ko, C. H. Jackman, R. A. Plumb, J. A. Kaye, and K. H. Sage (editors), Models and measurements intercomparison II, NASA/TM-1999-209554, 1999.

Pindyck, Robert S. and Daniel L. Rubinfeld, Econometric models and econometric forecastings, 4th ed., McGraw-Hill, 1998.

Popp, P. J., et al., Severe and Extensive Denitrification in the 1999-2000 Arctic Winter Stratosphere, *Geophys. Res. Lett.*, *28* (15), 2875-2878, 2001.

Reinsel, G. C., et al., Trend analysis of total ozone data for turnaround and dynamical contributions, *J. Geophys. Res*. *110*, D16306, doi:10.1029/2004JD004662, 2005.

Reinsel, G., E. Weatherhead, G. Tiao, A. Miller, R. Nagatani, D. Wuebbles, and L. Flynn, On detection of turnaround and recovery in trend for ozone, *J. of Geophys. Res.*, *107*, 1-1 - 1-12, 2002.

Reinsel, G.C., Trend analysis of upper stratospheric Umkher ozone data for evidence of turnaround, *Geophys. Res. Lett.*, *29* (10), 91-1 to 91-4, 2002.

Reinsel, G.C., G.C. Tiao, D.J. Wuebbles, J.B. Kerr, A.J. Miller, R.M. Nagatani, L. Bishop, and L.H. Ying, Seasonal trend analysis of published ground-based and TOMS total ozone data through 1991, *J. Geophys. Res.*, *99* (D3), 5449-5464, 1994.

Rex, M., R. J. Salawitch, P. Gathen, N. R. P. Harris, M. P. Chipperfield, and B. Naujokat, Artic ozone loss and climate change, *Geophys. Res. Lett.*, *31*, L04116, 2004.

Rinsland, C. P., R. J. Salawitch, M. R. Gunson, S. Solomon, R. Zander, E. Mahieu, A. Goldman, M. J. Newchurch, F. W. Irion, and A. Y. Chang, Polar stratospheric descent of NO_y and

CO and Arctic denitrification during winter 1992 - 1993, *J. Geophys. Res*., *104*, 1847, 1999.

Robock, A., Volcanic eruptions and climate, *Rev. Geophys*., *38*, 191, 2000.

Russel III, J. M., et al., Validation of hydrogen chloride measurements made by the Halogen Occultation Experiment from the UARS platform, *J. Geophys. Res.*, *101* (D6), 10,151-10,162, 1996a.

Russell III, J. M., et al., Validation of hydrogen fluoride measurements made by the Halogen Occultation Experiment from the UARS platform, *J. Geophys. Res.*, *101* (D6), 10,163-10,174, 1996b.

Russell III, J.M., L.L. Gordley, J.H. Park, S.R. Drayson, W.D. Hesketh, R.J. Cicerone, A.F. Tuck, J.E. Frederick, J.E. Harries, and P.J. Crutzen, The Halogen Occultation Experiment, *J. Geophys. Res.*, *98* (D6), 10,777-10,797, 1993.

Salawitch, R. J., et al., The distribution of hydrogen, nitrogen, and chlorine radicals in the lower stratosphere: implications for changes in O_3 due to emission of NO_y from supersonic aircraft, *Geophys. Res. Lett*., *21*, 2547-2550, 1994.

Salawitch, R. J., et al., Chemical loss of ozone during the Arctic winter of 1999/2000: An analysis based on balloon-borne observations., *J. Geophys. Res.*, *107* (D20, 10.1029/2001JD000620), 8269-8289, 2002.

Salawitch R. J., D. K. Weisenstein, L. J. Kovalenko, C. E. Sioris, P. O. Wennberg, K. Chance, M. K. W. Ko, and C. A. McLinden, Sensitivity of ozone to bromine in the lower stratosphere, *Geophys. Res. Lett*., *32*, L05811, doi:10.1029/2004GL021504, 2005.

Salawitch, R. J., Atmospheric Chemistry – Biogenic Bromine, *Nature*, *439*, 275–277, 2006.

Santer, B. D., et al., Contributions of anthropogenic and natural forcing to recent tropopause height changes, *Science*, *301*, 479, 2003.

Sen, B., et al., The budget and partitioning of stratospheric chlorine during the 1997 Arctic summer, *J. Geophys. Res.*, *104* (D21), 26,653-26,665, 1999.

Sen, B., G. C. Toon, G. B. Osterman, J. -F. Blavier, J. J. Margitan, and R. J. Salawitch, Measurements of reactive nitrogen in the stratosphere, *J. Geophys. Res.*, *103* (D3), 3571-3585, 1998.

Shindell, D. T., D. Rind, and P. Lonergan, Increased polar stratospheric ozone losses and delayed eventual recovery owing to increasing greenhouse-gas concentrations, *Nature*, *392*, 589-592, 1998.

Sinnhuber, B.-M., A. Rozanov, N. Sheode, O.T. Afe, A. Richter, M. Sinnhuber, F. Wittrock, J.P. Burrows, G.P. Stiller, T. von Clarmann, and A. Linden, Global observations of stratospheric bromine monoxide from SCIAMACHY, *Geophys. Res. Lett.*, *32*, L20810, doi:10.1029/2005GL023839, 2005.

Sioris, C. L. J. Kovalenko, C. A. McLinden, R. J. Salawitch, M. Van Roozendael, F. Goutail, M. Dorf, K. Pfeilsticker, K. Chance, C. von Savigny, X. Liu, T. P. Kurosu, J.-P. Pommereau, H. Bösch, and J. Frerick, Latitudinal and vertical distribution of bromine monoxide in the lower stratosphere from SCIAMACHY limb scattering measurements, *J. Geophys. Res.*, submitted, 2006.

Slusser, J., J. Gibson, D. Bigelow, D. Kolinski, W. Mou, G. Koenig, and A. Beaubien, Comparison of column ozone retrievals by use of an UV multifilter rotating shadow-band radiometer with those from Brewer and Dobson spectrophotometers, *Applied Optics*, *38* (9), 1543-1551, 1999.

Solomon, S., R.W. Portmann, T. Sasaki, D.J.Hofmann, and D.W.J. Thompson, Four decades of ozonesonde measurements over Antarctica, *J. Geophys. Res.*, *110*, D21311, doi:10.1029/2005JD005917, 2005.

SPARC, Assessment of Upper Tropospheric and Stratospheric Water Vapour, in *WMO*, edited by D. Kley, Russell, J. M., and Phillips, C., pp. 312, Geneva, 2000.

Staehelin, J., A. Renaud, J. Bader, R. McPeters, P. Viatte, B. Hoegger, V. Bugnion, M. Giroud, and H. Schill, Total ozone series at Arosa (Switzerland): Homogenization and data comparison, *J. Geophys. Res.*, *103* (D5), 5827-5841, 1998.l jurk

Staehelin, J., H. Schill, B. Högger, P. Viatte, G. Levrat, and A. Gamma, Total ozone observation by sun photometry at Arosa, Switzerland, *Opt. Engin.*, *34*, 1977-1986, 1995.

Steinbrecht, W., et al., Inteannual variation patterns of total ozone and temperature in observations and model simulations, *Atmos. Chem. Phys*. *Discuss*., *5*, 9207-9248, 2005.

Stolarski, R. S., P. Bloomfield, R. D. McPeters, and J. R. Herman, Total ozone trends deduced from Nimbus 7 TOMS data, *Geophys. Res. Lett.*, *18*, 1015-1018, 1991.

Thomason, L. W. and L. R. Poole, A global climatology of stratopsheric aerosol surface area density deduced from Stratospheric Aerosol and Gas Experiment II measurements: 1984-1994, *J. Geophys. Res.*, *102* (D7), 8967-8976, 1997.

Tilmes, S., R. Müller, J.-U. Grooß, and J. M. Russell III, Ozone loss and chlorine activation in the Arctic winters 1991-2003 derived with the tracer-tracer correlation, *Atmos. Chem. Phys*., *4*, 2181-2213, 2004.

Wamsley, P. R., et al., Distribution of halon-1211 in the upper troposphere and lower stratosphere and the 1994 total bromine budget, *J. Geophys. Res.*, *103* (D1), 1513-1526, 1998.

Wang, H. J., D. M. Cunnold, L. W. Thomason, J. M. Zawodny, and G. E. Bodeker, Assessment of SAGE version 6.1 ozone data quality, *J. Geophys. Res.*, *107* (D23), 8-1 to 8-18, 2002.

Waugh, D. W., D. B. Considine, and E. L. Fleming, Is upper stratospheric chlorine decreasing as expected?, *Geophys. Res. Lett.*, *28*(7), 1187-1190, 2001.

Weatherhead, E.C, and S. B. Andersen, The search for signs of ozone recovery, Nature, *submitted*, 2005

Wennberg, P. O., et al., Removal of stratospheric ozone by radicals: in situ measurements of OH, HO_2, NO, NO_2, ClO, and BrO, *Science*, *266*, 398-404, 1994.

WMO, Scientific Assessment of Ozone Depletion: 1994 - Ozone Measurements, in *World Meteorological Organization*, pp. 54, Washington, D.C., 1994.

WMO, Scientific Assessment of Ozone Depletion: 1998, in *NASA, NOAA, UNEP, WMO, EC*, pp. 1-44 pp., Geneva, Switzerland, 1999.

WMO, Global ozone research and monitoring project, Report No. 47, in *Scientific assessment of ozone depletion: 2002*, Geneva, Switzerland, 2003.

Woodbridge, E. L., et al., Estimates of total organic and inorganic chlorine in the lower stratosphere from in situ and flask measurements during AASE II, *J. Geophys. Res.*, *100* (D2), 3057-3064, 1995.

Yang, E.-S., D. M. Cunnold, M. J. Newchurch, R. J. Salawitch, Change in ozone trends at southern high latitudes, *Geophys. Res. Lett.*, *32*, L12812, doi:10.1029/2004GL022296, 2005.

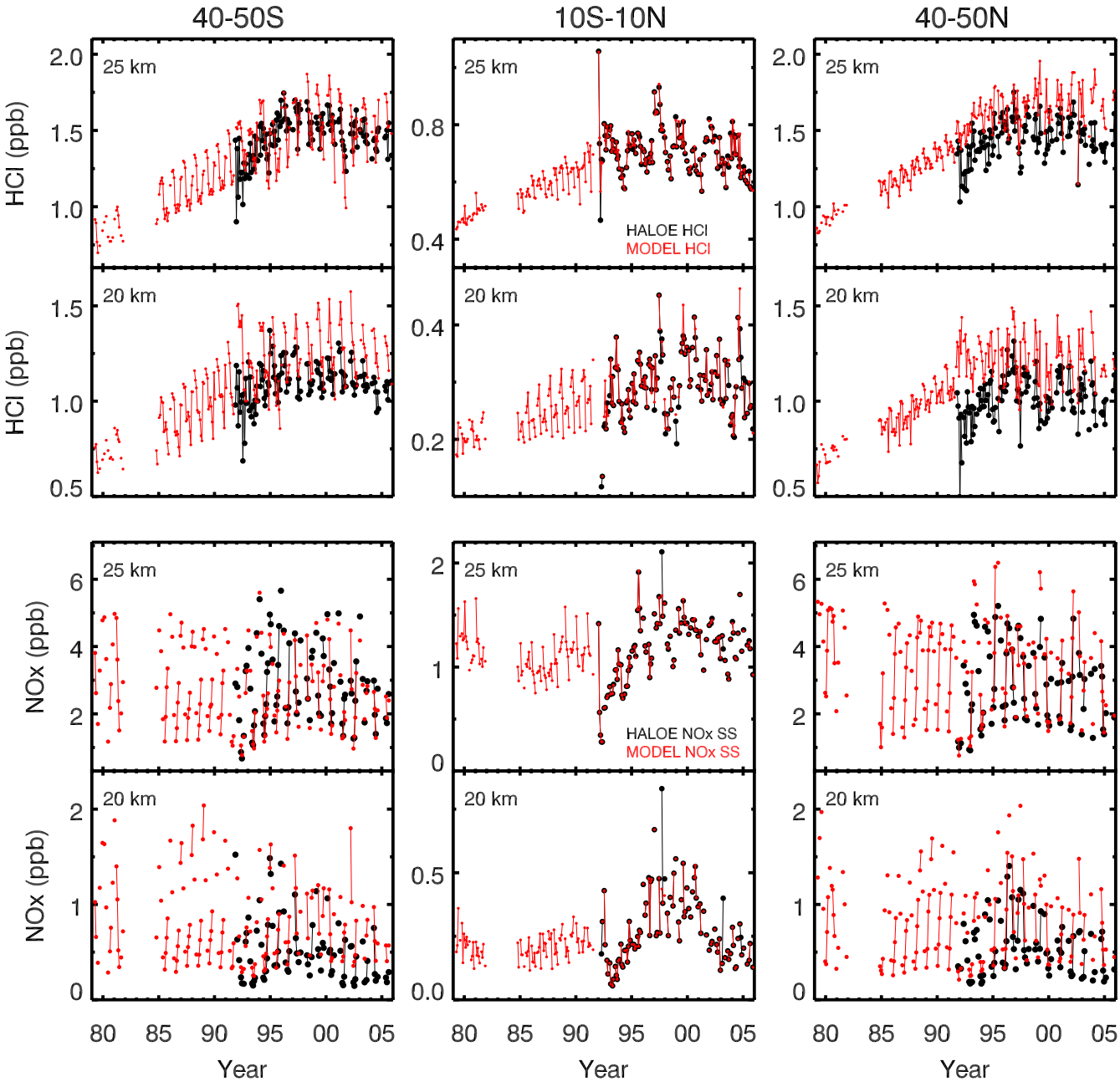
40-50S
10S-10N
40-50N
25 km
20 km
HCl (ppb)
NOx (ppb)
HALOE HCl
MODEL HCl
HALOE NOx SS
MODEL NOx SS
Year
80
85
90
95
00
05

Figure 1

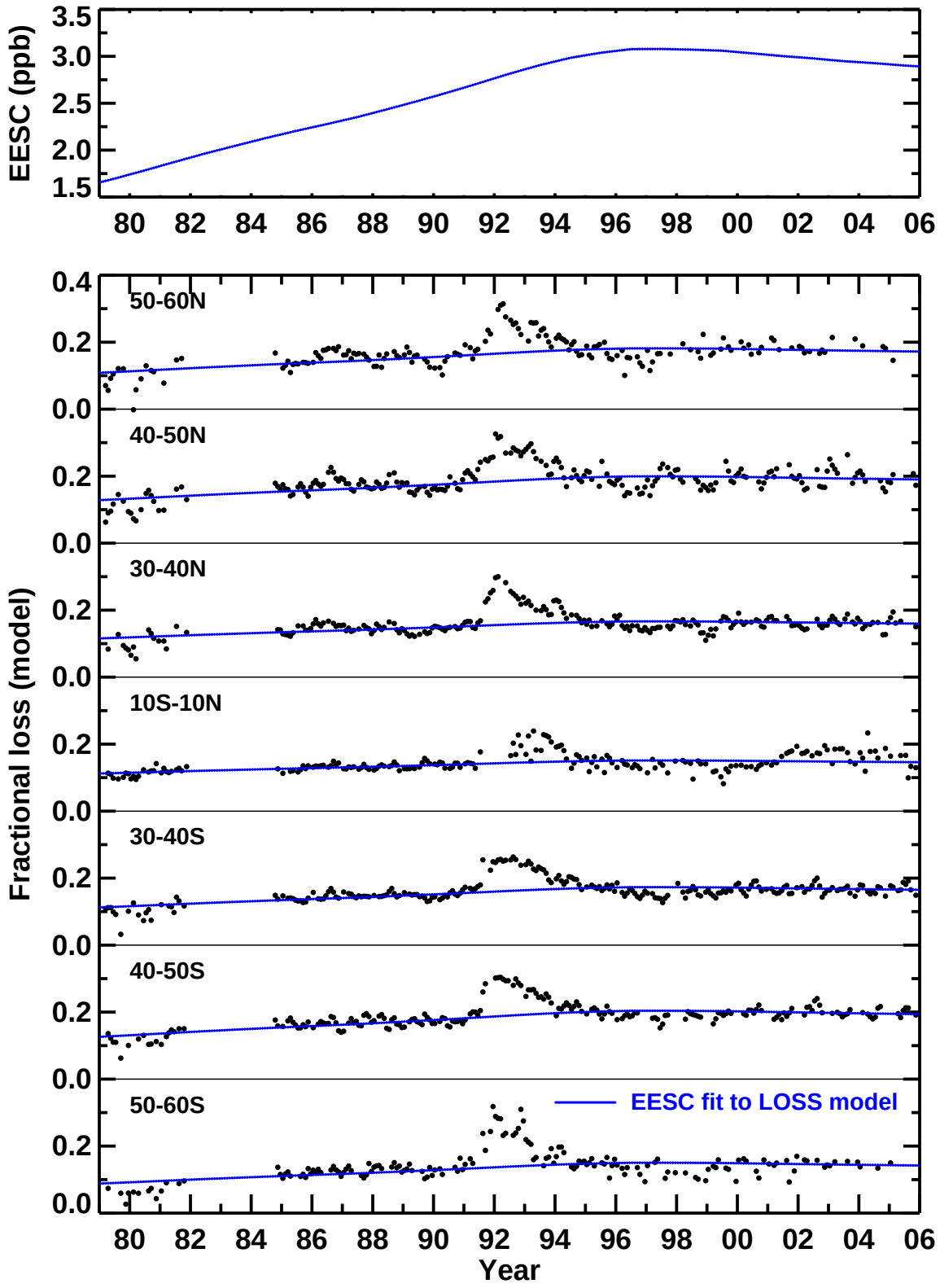
EESC (ppb)
3.5
3.0
2.5
2.0
1.5
80 82 84 86 88 90 92 94 96 98 00 02 04 06
Fractional loss (model)
50-60N
40-50N
30-40N
10S-10N
30-40S
40-50S
50-60S
0.4
0.2
0.0
EESC fit to LOSS model
Year

Figure 2

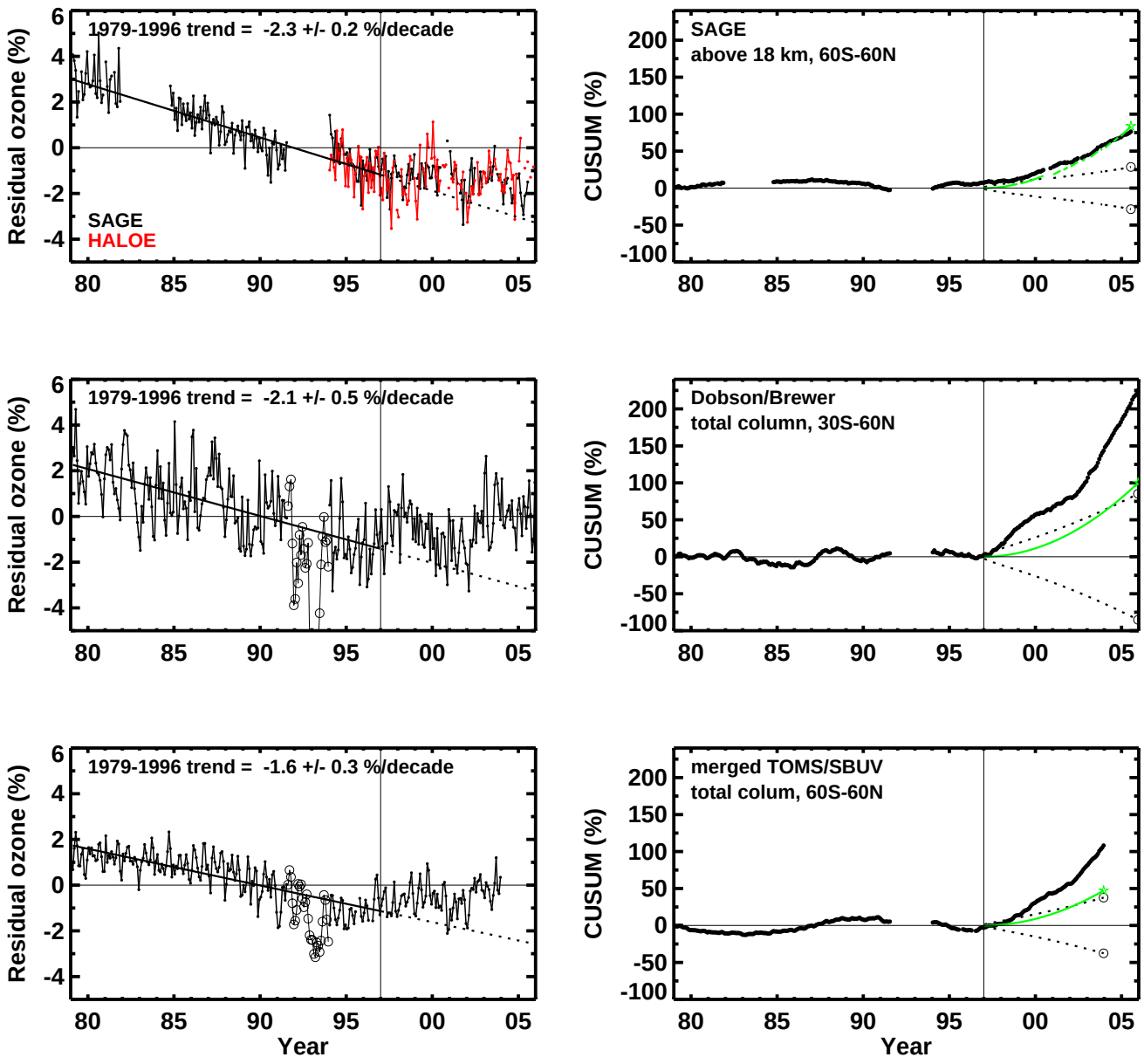
1979-1996 trend = -2.3 +/- 0.2 %/decade
SAGE
HALOE
Residual ozone (%)
SAGE
above 18 km, 60S-60N
CUSUM (%)
1979-1996 trend = -2.1 +/- 0.5 %/decade
Residual ozone (%)
Dobson/Brewer
total column, 30S-60N
CUSUM (%)
1979-1996 trend = -1.6 +/- 0.3 %/decade
Residual ozone (%)
merged TOMS/SBUV
total colum, 60S-60N
CUSUM (%)
Year
Year

Figure 3

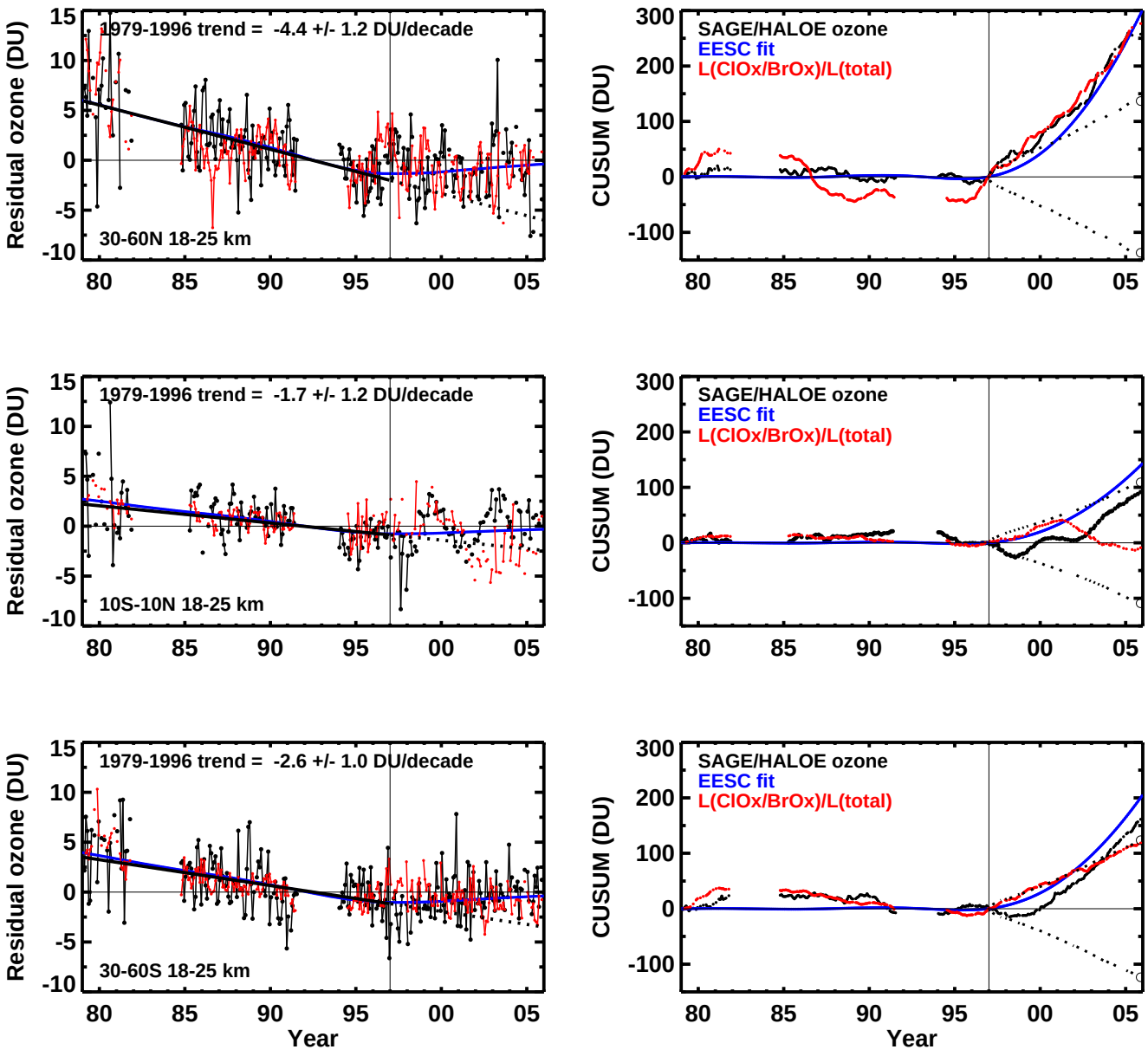
1979-1996 trend = -4.4 +/- 1.2 DU/decade
30-60N 18-25 km
1979-1996 trend = -1.7 +/- 1.2 DU/decade
10S-10N 18-25 km
1979-1996 trend = -2.6 +/- 1.0 DU/decade
30-60S 18-25 km
Residual ozone (DU)
SAGE/HALOE ozone
EESC fit
L(ClOx/BrOx)/L(total)
CUSUM (DU)
Year

Figure 4

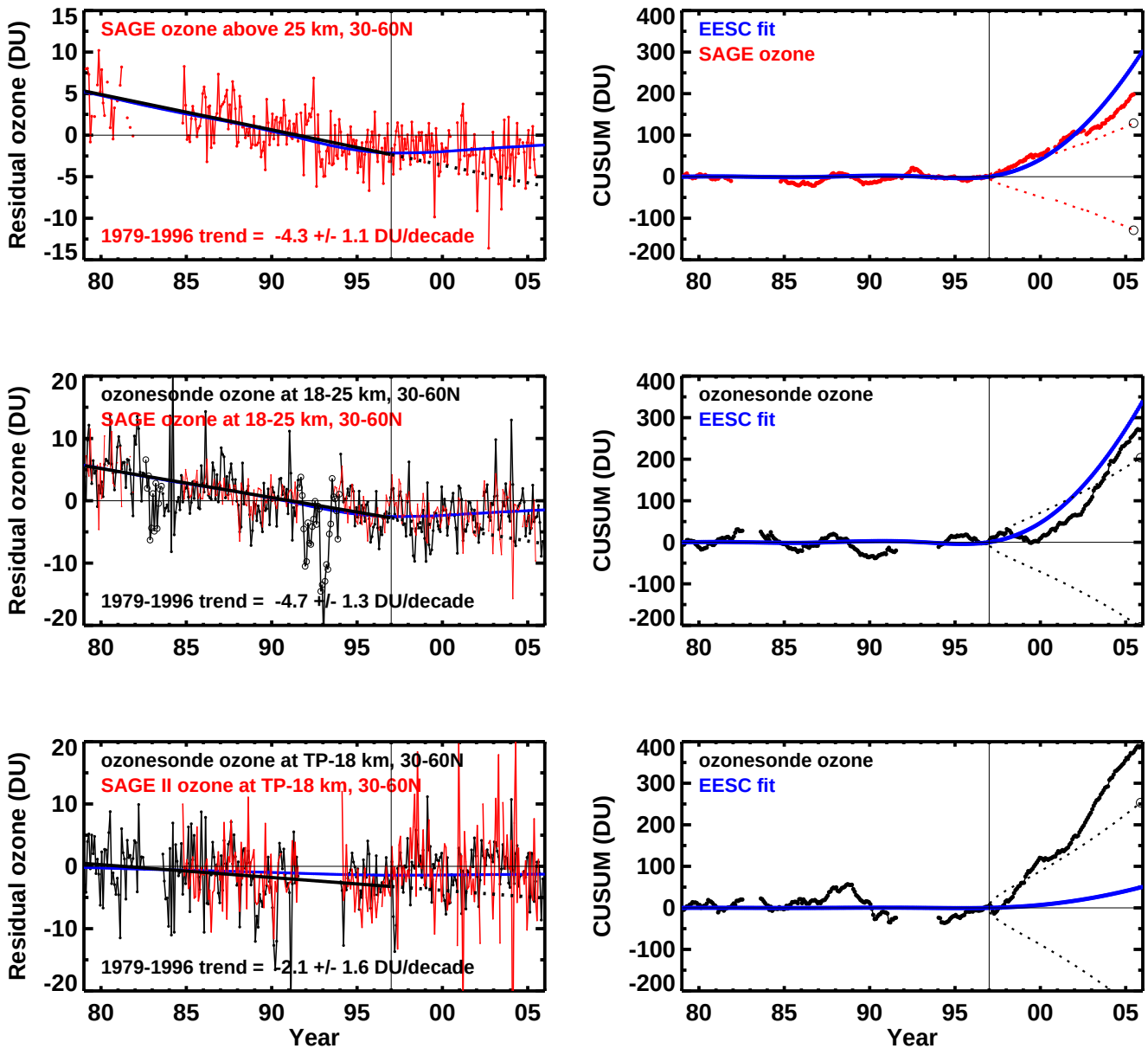
SAGE ozone above 25 km, 30-60N
1979-1996 trend = -4.3 +/- 1.1 DU/decade
Residual ozone (DU)
EESC fit
SAGE ozone
CUSUM (DU)
ozonesonde ozone at 18-25 km, 30-60N
SAGE ozone at 18-25 km, 30-60N
1979-1996 trend = -4.7 +/- 1.3 DU/decade
ozonesonde ozone
EESC fit
ozonesonde ozone at TP-18 km, 30-60N
SAGE II ozone at TP-18 km, 30-60N
1979-1996 trend = -2.1 +/- 1.6 DU/decade
Year

Figure 5

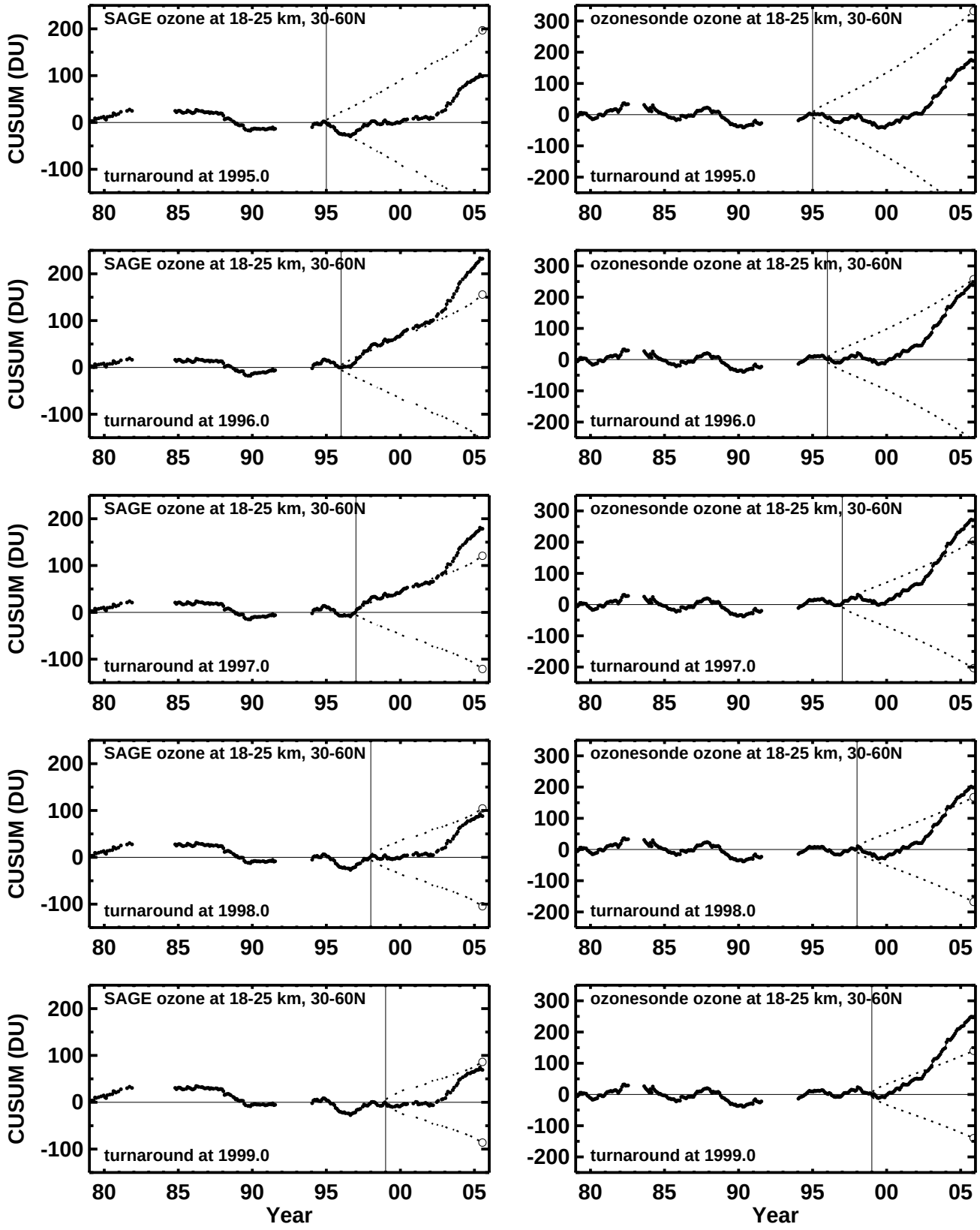
SAGE ozone at 18-25 km, 30-60N
ozonesonde ozone at 18-25 km, 30-60N
turnaround at 1995.0
turnaround at 1996.0
turnaround at 1997.0
turnaround at 1998.0
turnaround at 1999.0
CUSUM (DU)
Year
80
85
90
95
00
05

Figure 6

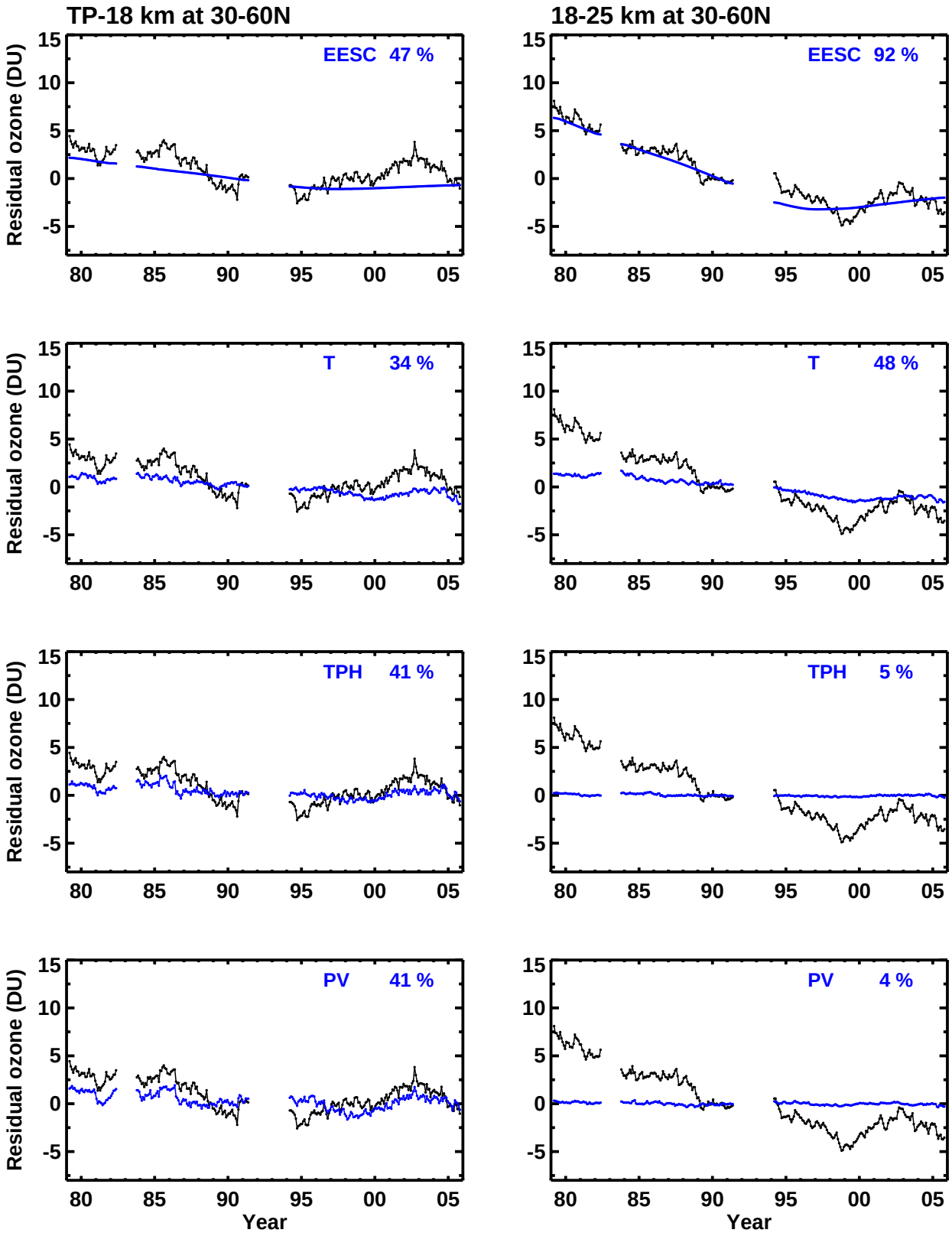
TP-18 km at 30-60N
18-25 km at 30-60N
EESC 47 %
EESC 92 %
T 34 %
T 48 %
TPH 41 %
TPH 5 %
PV 41 %
PV 4 %
Residual ozone (DU)
Year
15
10
5
0
-5
80
85
90
95
00
05

Figure 7

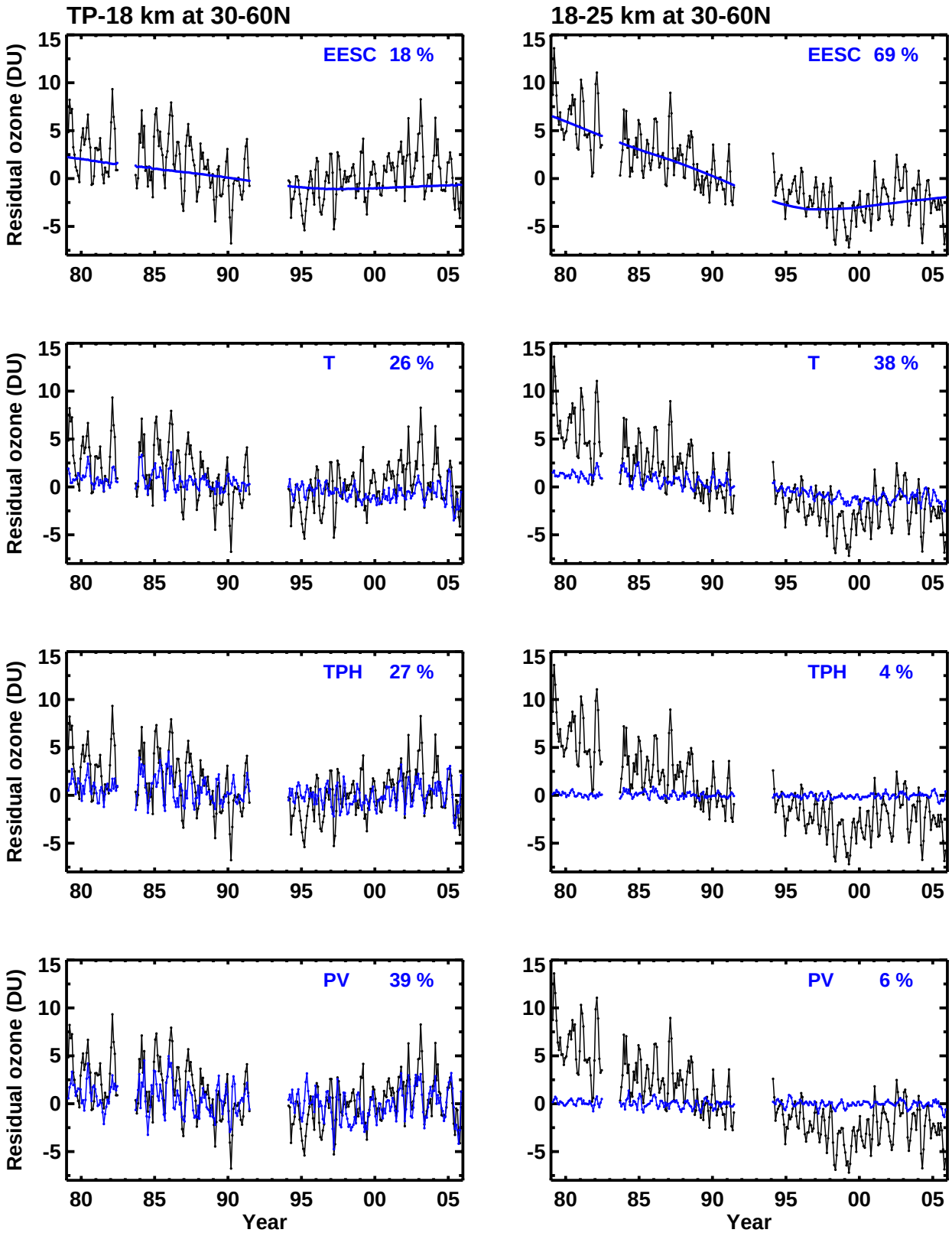
TP-18 km at 30-60N
18-25 km at 30-60N
EESC 18 %
EESC 69 %
T 26 %
T 38 %
TPH 27 %
TPH 4 %
PV 39 %
PV 6 %
Residual ozone (DU)
Year
15
10
5
0
-5
80
85
90
95
00
05

Figure 8

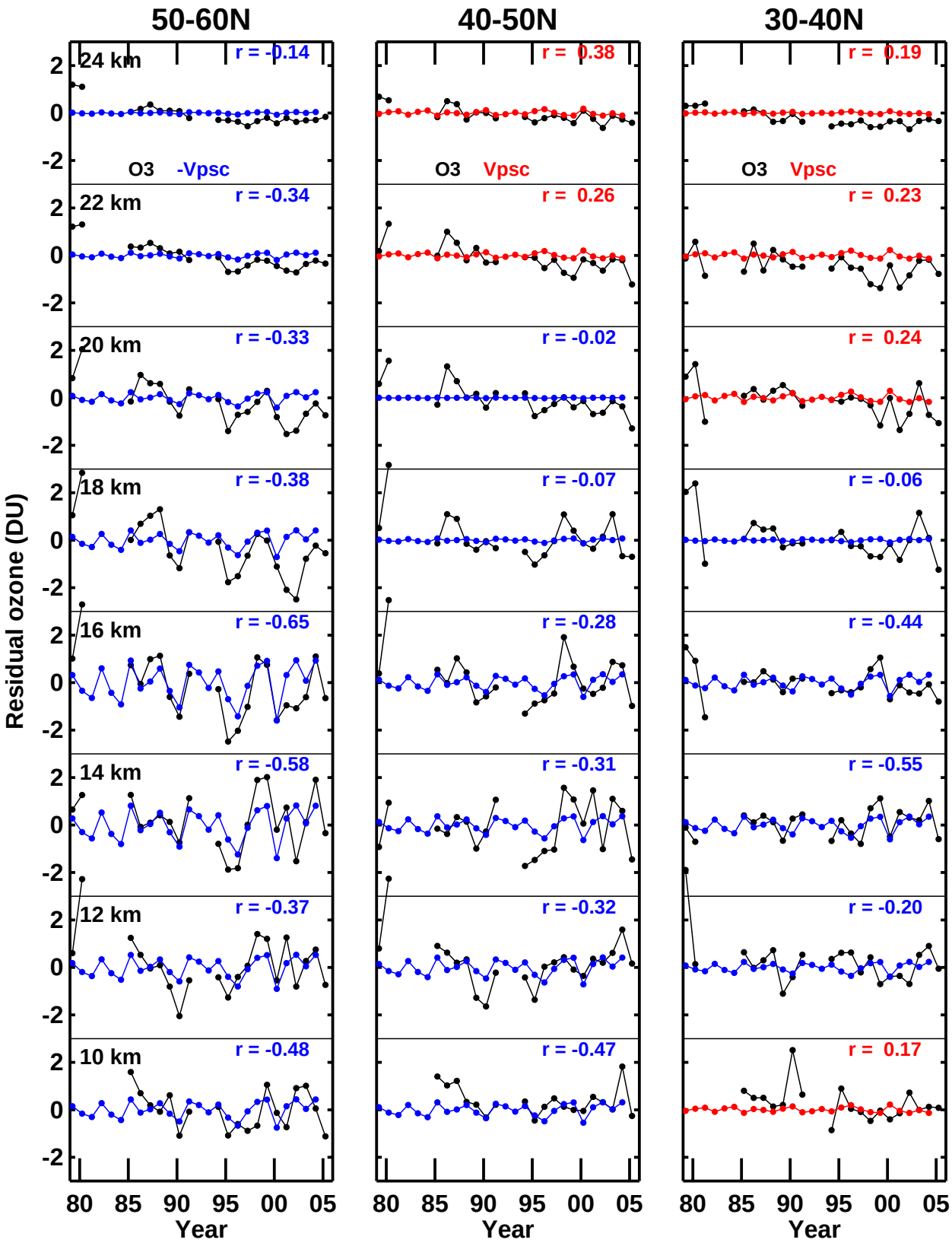
50-60N
40-50N
30-40N
24 km
22 km
20 km
18 km
16 km
14 km
12 km
10 km
r = -0.14
r = -0.34
r = -0.33
r = -0.38
r = -0.65
r = -0.58
r = -0.37
r = -0.48
r = 0.38
r = 0.26
r = -0.02
r = -0.07
r = -0.28
r = -0.31
r = -0.32
r = -0.47
r = 0.19
r = 0.23
r = 0.24
r = -0.06
r = -0.44
r = -0.55
r = -0.20
r = 0.17
O3 -Vpsc
O3 Vpsc
O3 Vpsc
Residual ozone (DU)
2
0
-2
80 85 90 95 00 05
Year

Figure 9